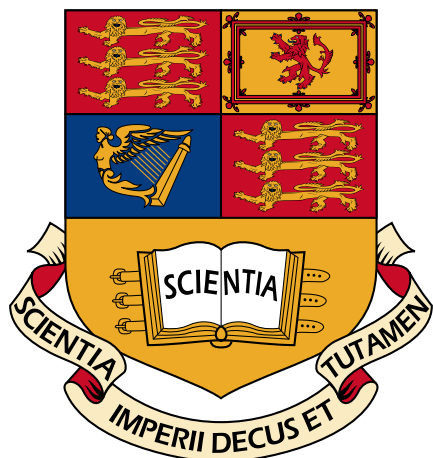


Imperial College London

Department of Electrical and Electronic Engineering

Final Year Project Report 2020



Project Title: **Energy Harvesting from Water Flow**

Student: **Alexander Adolfsson**

CID: **01831271**

Course: **ELEC97031**

Project Supervisor: **Prof. Andrew Holmes**

Second Marker: **Prof. Richard Syme**

Abstract

Harvesting the energy directly from the water flow in a continuous and reliable way to power the water leakage monitoring systems is a way to reduce the dependency on batteries. The purpose of this research is to construct a small hydropower turbine which can easily be installed in smaller pipes. There were two different turbine types designed and tested. An impulse turbine design based on the Pelton wheel and a reaction turbine design based on Darrieus water turbine. The generator was of the axial flux permanent magnet design and constructed by hand. The turbine parts were 3D printed and then manually assembled with the generator. The results of the test showed that the reaction turbine design didn't manage to rotate in the tested flow velocity, but the impulse turbine design started to rotate continuous from around a flow velocity of 1 m/s. The impulse turbines produced a maximum power of $340mW$ with its highest efficiency of 0.022 at $RPM = 2240$. The low efficiency and RPM values resulted in that the generators output voltage and current could not be measured using a Multimeter for any flow velocity making the generators efficiency unknown.

Acknowledgements

I would like to thank Prof. Andrew Holmes for the support and guidance he have provided as supervisor during this project. This project would not be possible without his expertise in the area and I have had many rewarding meetings and conversations with him. I would also like to thank Prof. Richard Syms whom helped me understand the necessary background theory.

Contents

1	Introduction	1
2	Background	3
2.1	Fluid Mechanics	3
2.1.1	Energy Equations	3
2.2	Impulse Water Turbine	4
2.2.1	Power Generated	6
2.3	Reaction Water Turbine	6
2.3.1	Steam Tube Model	6
2.3.2	Calculate Values Using the Model	8
2.3.3	Optimisation	8
2.4	Axial Flux Permanent Magnet Generator	9
2.4.1	General Design	9
2.4.2	Non-Overlap Windings	9
2.4.3	Magnetic Flux	11
2.4.4	EMF	11
2.4.5	PM Halbach Array	12
2.4.6	Losses	12
2.4.7	Power System	15
3	Requirements	18
3.1	Requirement of the Generator	18
3.2	Requirement of the Turbine	18
4	Analysis and Design	20
4.1	Impulse Turbine Design	20
4.2	Reaction Turbine Design	20
4.3	Generator Design	21
4.4	Complete Construction	23
5	Implementation	28
5.1	Designing	28
5.2	Constructing	29
6	Testing	33
6.1	Testing Rig	33
6.2	Method	34
7	Results	37
7.1	Impulse Turbine Results	37
7.2	Reaction Turbine Results	38
8	Conclusions and Further Work	40
8.1	Evaluation	40
8.2	Turbine Conclusion	41
8.3	Generator Conclusion	42
8.4	Further Work	43

List of Tables

3.1	Specification for the hydropower system	19
4.1	Stator coil variables	23
6.1	Water Pump Specification	33
6.2	The water flows are based on figure 6.1 and not a formula or measurement. Therefore the exact flow values may differ from the ones in the table.	36
7.1	The turbine RPM calculated for video footage.	37
7.2	The turbine power and efficiency calculated.	37

List of Figures

2.1	Shows typical arrangement of a Pelton wheel turbine.	5
2.2	Pelton wheel bucket shape.	5
2.3	Star connected three phase diagram.	16
2.4	Phasor diagram.	16
2.5	Phasor diagram with the load impedance.	17
4.1	Impulse turbine blades top view.	21
4.2	Impulse turbine.	22
4.3	Airfoil NACA 0015 shape.	22
4.4	Reaction turbine blades top view.	23
4.5	Reaction turbine.	24
4.6	Lift and drag graphs for airfoil NACA 0015 at Reynolds number $Re = 50000$	25
4.7	Generator view.	26
4.8	Power as a function of load at 30000 RPM.	26
4.9	Reaction turbine design.	27
4.10	Impulse turbine design.	27
5.1	Power from flow interacting on the impulse turbine.	29
5.2	Iterative flowchart to calculate the flow velocity.	30
5.3	Graph of power coefficient based on TSR.	31
5.4	Graphs of reaction turbines output values at $\lambda = 2$	31
5.5	Iterative flowchart to calculate the values of the axial flux PMSG.	32
5.6	Graphs of output values at tangential velocity matches flow velocity.	32
6.1	Water Pump Flow Chart	34
6.2	Flow Rig	35
6.3	Inserted hydropower turbine	35
7.1	Impulse turbine results.	38
7.2	Impulse turbine connected in the pipe at a -15° angle.	39
A.1	Impulse turbine support structure design schematics in mm.	48
A.2	Reaction turbine support structure design schematics in mm.	49
A.3	Impulse turbine design schematics in mm.	50
A.4	Reaction turbine design schematics in mm.	51

Chapter 1

Introduction

The water distribution network is an extensive system of pipes running across the entire country. To make sure that everything is working correctly much data is gathered using sensors on or in the water pipes. One way that sensors are utilised is to detect water leakages in the distribution network that can then be repaired. One issue that Chartered Institution of Water and Environmental Management (CIWEM) raised was the time to find and fix leakages. A solution proposed was new sensory technology that could find leakages faster but they also had to be economically justified [1]. The way to reduce the time to find leakages can be new techniques or increasing the number of sensors. Another reason for increasing the amount of sensors are to test different parameters, such as the quality of drinking water, which was requested by the U.S. Environmental Protection Agency (EPA) [2] to better monitor the water quality of their drinking water.

The biggest issue with installing sensors on water distribution system is the need to power the sensors. The distribution networks are very large and can be hard to access, making installation of sensors problematic as drawing a power wire is not always the easiest. It is therefore desirable to install self powering sensors. The self powering sensor harvest energy from the water flow using turbines that power the sensor equipment. This is an active topic and several recent researches have been done on different possible models [3, 4, 5]. The problems with most self powering sensors is the installation that require modifications to existing pipes such as the products offered by the company Pydro or the models proposed by [5]. These models require are best implemented on new construction or where it's easy to drain and modify existing pipes. Another issue is that each model only fits one size of pipe diameter. This is not that big of a problem because of standardised diameters but does increase the cost of the manufacturer.

There have been some important advancements made during the last decade that enable the designing and construction of very small-scale energy harvester to be simple and cheap. The first one is the advancement of 3D printing which enables the complicated designs to easily be constructed. An other advancement is the research in the axial flux permanent magnetic generators and their advantages over the more classical radial flux generator as studied by [6]. The axial flux generator have an advantages in efficiency for small scale applications compared

to the radial because of its geometrical design. Researches by [7] have shown that axial flux micro generator have demonstrated much higher power density then even macro generator.

The project work aims to develop a small and cheap energy harvester that can generate enough energy to power a sensor. Its installation into water pipes are to be easy both for older ones currently in use but also for new ones being built.

Chapter 2

Background

The background theory necessary is divided among the four main parts, fluid mechanics, impulse water turbine, reaction water turbine, and synchronous generator. As these are very large areas covered, only the specific knowledge needed to understand and construct the energy harvester is described and when simplifications or assumptions are made it's clearly stated and reasoned why it can be done.

2.1 Fluid Mechanics

The flow of water in pipes can be either laminar or turbulent dependent on several factors according to [8] where if the Reynolds number exceeded a critical value the flow would be turbulent. The critical value varied greatly, from 2300 to 40000, dependent on the disturbance in the incoming flow, a smaller disturbance would increase the critical Reynolds number. The formula for calculating Reynolds number for round pipes stated by [9] is

$$Re = \frac{d\dot{V}/A}{\nu} \quad (2.1)$$

where d is the pipe diameter, \dot{V} is the volume flux, A is the pipe cross-sectional area, and ν is the kinematic viscosity of the fluid. The flow in the pipe will be turbulent flow because of its small cross-sectional area and high-water flow, resulting in a Reynolds number higher than the critical range for turbulent flow. The velocity distribution for turbulent flow in pipes is almost uniformly in the centre part of the pipe while the borders, close to the walls, have a lower velocity. An assumption made to make calculations easier is to assume a constant velocity uniformly spread over the entire cross-section of the pipe.

2.1.1 Energy Equations

The total energy in turbulent flow \tilde{e}_{tot} per volume is given in the equation from [9] as

$$\tilde{e}_{tot} = \tilde{e} + \frac{1}{2}(\tilde{u}^2 + \tilde{v}^2 + \tilde{w}^2) + \frac{1}{2}(\widetilde{u'' * u''} + \widetilde{v'' * v''} + \widetilde{w'' * w''}) \quad (2.2)$$

and

$$u = \tilde{u} + u'', \quad v = \tilde{v} + v'', \quad w = \tilde{w} + w'' \quad (2.3)$$

where \tilde{e} is the average internal energy, u, v, w are the flow velocity vectors, $\tilde{u}, \tilde{v}, \tilde{w}$ are the average flow velocity vectors, and u'', v'', w'' are the flow velocity fluctuations. This can be simplified to calculate the energy passing through the turbine. The average internal energy can be assumed to be a constant, this is because of the large difference between the total energy and the energy converted by the turbine. The flow in the pipes only have one direction and therefore reduces the three-dimensional problem into a single dimension. To simplify the equation further the fluctuation in velocity will be ignored. The simplification will result in an inaccurate energy equation however a more precise method would be difficult to calculate without advanced simulation or measurement equipment. The kinetic energy in the flow per volume is then

$$K = \frac{1}{2}u^2. \quad (2.4)$$

The power of the water can then be calculated using the flow rate $Q = V/s$ as

$$P_{flow} = \rho Q K = \frac{1}{2}\rho A_{turbine} u^3 \quad (2.5)$$

where $A_{turbine}$ is area of the turbine facing the flow and ρ is the fluid density.

2.2 Impulse Water Turbine

Impulse water turbine generates torque from the kinetic energy from the water flow, not the pressure difference as some other water turbines. The most common example is the Pelton wheel, see figure. 2.1 water turbine which is only partially connected to the water stream in the lower part, leaving most of the wheel in the air. This enables it to extract more energy from the water as the resistance from the air on the upper side is much lower than the force from the water. The same method can be used for a turbine fully submerged in the water by blocking the water flow from the top part of the turbine, which minimises the counter torque affecting it.

The blade design of the turbine is shaped as a bucket to capture as much water as possible. While the Pelton wheel strives to redirect the water hitting the blades, maximising the power transferred, by designing the blade into two buckets, see figure 2.2, and having the water jet hitting the intersection of the buckets. The same approach is not desirable for this scale when the water flow can not be directed, therefore the blade itself will be smooth and not redirect the water flow. A study by [10] shows that to maximise the torque of the turbine, by increasing the volume of water contained, the blade should have baffle plates on both the top and bottom part.

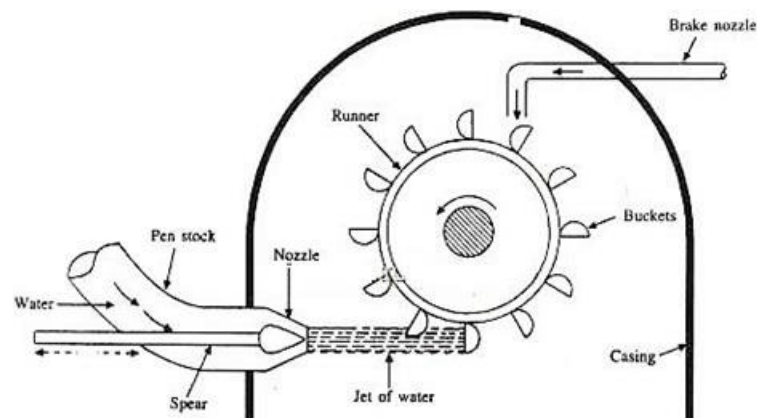


Figure 2.1: Shows typical arrangement of a Pelton wheel turbine.

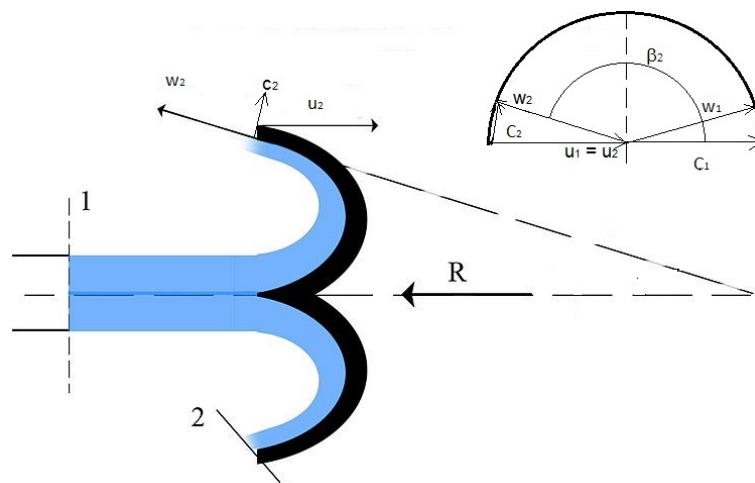


Figure 2.2: Pelton wheel bucket shape.

2.2.1 Power Generated

The turbines efficiency is easiest to calculate using the power from the generator together with the power from the water flow

$$\eta = \frac{P_{el}}{P_{flow}} \quad (2.6)$$

where P_{el} is the power from the generator and P_{flow} is the power from the water passing through the turbine, see equation 2.5. To calculate the efficiency of only the turbine without the generator, i.e.

$$\eta = \frac{P_{turbine}}{P_{flow}} \quad (2.7)$$

where the turbine power $P_{turbine}$ is

$$P_{turbine} = F_t \times v_t \quad (2.8)$$

where F_t is the tangential force on the turbine and v_t its tangential velocity. The tangential force is

$$F_t = ma_t = \frac{mv_t^2}{r} = mr\omega^2 \quad (2.9)$$

where m is the turbines mass, r its radius, and ω is its angular velocity. The turbine power can then be expressed as

$$P_{turbine} = mr\omega^2 \times v_t = mr^2\omega^3. \quad (2.10)$$

2.3 Reaction Water Turbine

The vertical axis water turbine (VAWT) is a type of reaction turbine that is also called the Darrieus water turbine for straight blades or Gorlov helical turbine for twisted blades. The main reason that the VAWT is used is because its height can be greater than its width and the rotating axis is on the same plane as the generator which simplifies the overall design. This turbine shares many similarities to the vertical axis wind turbine and much of the calculations is the same.

2.3.1 Steam Tube Model

One of the ways to calculate the power coefficient of a VAWT is using the momentum model. This method is mostly used for wind turbines but works for water turbine as long as the tip speed ratio (TSR) and solidity is not high [11]. The method to utilise this model is explained by [12]. The model assumes that the incoming flow velocity only comes from one direction and is perpendicular to the turbine. This model also assumes that each

blade is independent, i.e. they do not interfere with each other, and therefore only calculate with one blade and multiplies the results in the end with the total number of blades. This is a simplification that gives a more optimistic results than more advanced models. The velocity of the blade can be calculated as

$$V_R = \sqrt{(V_a \sin \theta)^2 + (V_a \cos \theta + \omega r)^2} \quad (2.11)$$

where V_a is the induced velocity, θ is the azimuth angle, ω is the rotational velocity, and r is the turbine radius. The equation can be normalised relative the free stream, $V_a = V_\infty(1 - a)$, into

$$\frac{V_R}{V_\infty} = \sqrt{((1 - a) \sin \theta)^2 + ((1 - a) \cos \theta + \lambda)^2} \quad (2.12)$$

where V_∞ is the flow velocity, a is the induction factor, and λ is the TSR

$$\lambda = \frac{\omega r}{V_\infty}. \quad (2.13)$$

The flow angle is expressed as

$$\phi = \arctan \left(\frac{(1 - a) \sin \theta}{(1 - a) \cos \theta + \lambda} \right) \quad (2.14)$$

and the angle of attack is

$$\alpha = \phi - \phi_a \quad (2.15)$$

where ϕ_a is the blade incidence angle. The normal and tangential coefficient expressed using the flow angle are

$$C_n = C_l \cos \phi + C_d \sin \phi \quad (2.16)$$

$$C_t = C_l \sin \phi - C_d \cos \phi \quad (2.17)$$

where C_l and C_d are the lift and drag coefficient respectively. The thrust on a single blade at the angle θ is

$$T_\theta = \frac{1}{2} \rho V_R^2 h c (C_t \cos \theta - C_n \sin \theta) \quad (2.18)$$

where ρ is the water density, h is the blade height, and c is the chord length. The torque on a single blade at the angle θ is

$$Q_\theta = \frac{1}{2} \rho V_R^2 h c C_{tr} r. \quad (2.19)$$

To calculate the average thrust and power of the turbine a stream tube model is assumed. The blade path is

slit into several stream tubes along the incoming flow, each $\Delta\theta$ degrees between them relative the blade flight path. The width of each tube is therefore

$$\Delta z = r\Delta\theta \sin \theta \quad (2.20)$$

and the number of tubes is $m = \pi/\Delta\theta$. The average aerodynamic thrust by N blades can then be calculated by

$$C_T = \left(\frac{Nc}{2r} \right) \left(\frac{V_R}{V_\infty} \right)^2 \frac{2}{\pi} \left(C_t \frac{\cos \theta}{\sin \theta} - C_n \right) \quad (2.21)$$

and the average torque by N blades can be calculated using Eq. 2.19 as

$$Q = N \sum_{i=1}^{2m} \frac{Q_\theta}{2m}. \quad (2.22)$$

The power coefficient of the turbine can be calculated using Eq. 2.17 by

$$C_p = \sigma \lambda \sum_{i=1}^{2m} \frac{\left(\frac{V_r}{V_\infty} \right)^2 C_t}{2m} \quad (2.23)$$

where $\sigma = Nc/2r$ is the solidity of the rotor.

2.3.2 Calculate Values Using the Model

The way to calculate the induced velocity V_a and get the TSR to power coefficient C_p is explained by [12] as to first assume a value of the induction factor a . Then using the value calculate Eq. 2.12 to 2.21 and using the value of Eq. 2.21 to calculate the induction factor from the empirical Glauert relationship given by [13]

$$C_T = \begin{cases} 4a(1-a) & a < \frac{1}{3} \\ 4a(1 - \frac{1}{4}a(5 - 3a)) & a > \frac{1}{3} \end{cases} \quad (2.24)$$

and if the guessed value differs from the calculated one then use the new induction factor and recalculate the same equations. This method is used for each steam tube and the power coefficient can then be calculated by Eq 2.23.

2.3.3 Optimisation

One aspect to consider with VAWT is that it's not self starting for low values of solidity and TSR as stated by [14] but a higher solidity together with a higher TSR makes the VAWT self starting. Increasing the solidity also increases the power coefficient at low TSR as stated by [15] compared to lower solidity. There are different designs concerning the rotor blades of the VAWT. The most common types are the straight bladed design and

the helical blade design. The straight blade design usually have higher power coefficient as stated by [16] but the helical type extends the long-term life of the turbine. The downside is also an increase in manufacturing cost. A study by [17] found that the most optimal twist angle for helical blade design is 60°.

2.4 Axial Flux Permanent Magnet Generator

The generator design is an axial flux permanent magnet (AFPM) generator which have several advantages over the more common radial flux PM (RFPM) counterpart. The primary advantage the AFPM generator holds is its high-power density enable it to have a small size but instead require a higher RPM values.

2.4.1 General Design

The design of the AFPM generator is somewhat limited by the application as it must be both small and waterproof. The design therefore is single-sided AFPM with internal PM rotor. A double sided AFPM was not chosen, despite the advantages of it, because of the design limitations for the energy harvester to make it possible to construct by hand. The same reason applies to the stator which has non-overlap coil windings. A more complex winding would prove difficult to construct as well as requiring a dual- or multi-sided AFPM.

AFPM machines have in general a low air gap. However for slotted machines the mean magnetic flux density decreases in the air gap corresponding to a fictitious increase in the air gap expressed using the Carter coefficient explained by [18]

$$g' = gk_C \quad (2.25)$$

where g is the air gap and $k_C > 1$ is the Carter coefficient expressed as

$$k_C = \frac{t_1}{t_1 - \gamma g} \quad (2.26)$$

$$\gamma = \frac{4}{\pi} \left[\frac{b_{14}}{2g} \arctan \left(\frac{b_{14}}{2g} \right) - \ln \sqrt{1 + \left(\frac{b_{14}}{2g} \right)^2} \right] \quad (2.27)$$

where t_1 is the average slot pitch and b_{14} is the width of the slot opening.

2.4.2 Non-Overlap Windings

The stator windings in a generator can be configured in several different ways. For non-overlap single-layered windings there are several different rules that must me met depending on the how the coils is connected as is explained by [18]. If the windings have slotted iron cores then every second tooth is wound, also known as alternate teeth wound. If the winding is air-cored, then the coils is displaced in a pattern where each phase is in

succession with the same clockwise winding. The windings can be concentrated which means that the coils is parallel connected and there is only one coil per coil group ($z = 1$) or distributed where the coils is connected in series forming a coil group ($z = 2, 3\dots$). The number of stator coils in single-layer windings is

$$Q_c = s_1/2 \quad (2.28)$$

where s_1 is the number of stator slots. The windings can be divided into pole sections F which repeats itself in either negative or positive periodicity. To calculate the number of pole sections F the greatest common divisor (GCD) of the number of coils and poles

$$F = GCD(2p, Q_c) \quad (2.29)$$

where $2p$ is the number of poles. If $2p/F$ is even, then positive boundary conditions must be applied. If $2p/F$ is uneven then negative periodic boundary conditions are applied. The number of coils in a coil group can be found when F is known from Eq. 2.29 using the relationship

$$z = \frac{Q_c}{m_1 F} = \frac{n_c}{F} \quad (2.30)$$

where m_1 is the number of phases and n_c is the number of coils per phase, i.e.

$$n_c = \frac{s_1}{2m_1} = \frac{Q_c}{m_1}. \quad (2.31)$$

To have non-overlap windings there are a set of rules concerning the pole and slot combinations stated by [18]. These are:

- the number of poles must be even;
- the number of slots must be a multiple of the number of phases and must be even in the case of single layer windings;
- the number if coils and slots are equal in double layer windings; in single layer windings the number of coils is equal to half the number of slots;
- the number of coils in a coil group (z) must be an integer;
- the number of slots can not be equal to the number of poles [18, p. 39].

The fundamental space harmonic distribution factor calculated by [19] is

$$k_{d1} = \frac{\sin(\pi/2m_1)}{z\sin[\pi/(2m_1 z)]} \quad (2.32)$$

For iron-cored windings the fundamental space harmonic pitch factor is

$$k_{p1} = \sin\left(\frac{\pi p}{s_1}\right) \quad (2.33)$$

and for air-cored windings it is calculated by [20] to

$$k_{p1} = \sin\left(\frac{\pi p}{s_1}\right) \frac{\sin(\theta_{re}/2)}{\theta_{re}/2} \quad (2.34)$$

where θ_{re} can be calculated as approximate

$$\theta_{re} = \frac{r_{in}}{r_e} \frac{\pi}{3} \quad (2.35)$$

where r_{in} is the inner radius of the stator windings and $r_e = (r_{in} + r_{out})/2$. The winding factor is then

$$k_{w1} = k_{d1} k_{p1}. \quad (2.36)$$

The winding factor for concentrated winding is lower than distributed but the disadvantage can be mitigated according to [21] by using better combinations of pole and slots number.

2.4.3 Magnetic Flux

The magnetic flux of the generator can be calculated using the following equations and relationships according to [18]. The average magnetic flux density is

$$B_{avg} = \alpha_i B_{mg} \quad (2.37)$$

where B_{mg} is the peak value of the magnetic flux density and α_i differs for different waveform. For sinusoidal waveform $\alpha_i = 2/\pi$ and for square waveform $\alpha_i = 0.84$. The magnetic flux per pole is

$$\phi_f = \alpha_1 B_{mg} \frac{\pi}{2p} (R_{out}^2 - R_{in}^2) \quad (2.38)$$

where $R_{out} = 0.5D_{out}$ is the outer radius of the PMs and $R_{in} = 0.5D_{in}$ is the inner radius. To calculate the magnetic flux density from cube PM the following equation applies

$$B_{mg} = \frac{B_r}{\pi} \left[\arctan\left(\frac{l^2}{2z\sqrt{4z^2 + 2l^2}}\right) - \arctan\left(\frac{l^2}{2(l+z)\sqrt{4(l+z)^2 + 2l^2}}\right) \right] \quad (2.39)$$

where z is the airgap distance and B_r is the Residual magnetism of the PM.

2.4.4 EMF

The EMF at no load is according to [18]

$$e_f = 2\pi f N_1 k_{w1} \phi_f \cos(\omega t) \quad (2.40)$$

where N_1 is the number of turns per phase, ϕ_f is from Eq. 2.38, and k_{w1} is from Eq. 2.36. The EMF rms value is

$$E_f = \pi\sqrt{2}pN_1k_{w1}\phi_fn_s \quad (2.41)$$

where n_s is rotor speed in rpm.

2.4.5 PM Halbach Array

The Halbach array is a method to arrange the PM in a special order to increase the efficiency of the rotor and is most often used with core less rotor. The arrangement for a Halbach array is to rotate the PMs magnetic orientation 90° for each magnet, i.e. the orientation will follow this pattern North East South West and repeat, instead of the classical North South pattern. This method can make the AFPM machine easier to produce and still get over 90% efficiency as demonstrated by [22].

2.4.6 Losses

The different losses from the generator can be calculated as is shown by [18]. The d.c. current stator winding resistance per phase is

$$R_{1dc} = \frac{N_1l_{1av}}{a_p a_w \sigma s_a} \quad (2.42)$$

where σ is the electric conductivity, a_p is the number of parallel current connections, a_w is the number of parallel conductors, and l_{1av} is the average length of a turn which is calculated by

$$l_{av} = 2L_i + l_{in} + l_{out} \quad (2.43)$$

where L_i is the armature stack length, l_{in} is the length of the inner connection, and l_{out} is the length of the outer connection. The a.c. current resistance also include the skin-effect where the resistance becomes

$$R_1 \approx k_{1R}R_{1dc} \quad (2.44)$$

where k_{1R} is the skin-effect coefficient. For three-phase single-layer winding the skin-effect coefficient is in general

$$k_{1R} = \varphi_1(\xi_1) + \left(-\frac{1}{16}\right)\psi_1(\xi_1) \quad (2.45)$$

where

$$\varphi_1(\xi_1) = \xi_1 \frac{\sinh 2\xi_1 + \sin 2\xi_1}{\cosh 2\xi_1 - \cos 2\xi_1} \quad (2.46)$$

$$\phi_1(\xi_1) = 2\xi_1 \frac{\sinh \xi_1 - \sin \xi_1}{\cosh \xi_1 + \cos \xi_1} \quad (2.47)$$

$$\xi_1 = h_c \sqrt{\pi f \mu_0 \sigma_1} \quad (2.48)$$

and h_c is the conductor height.

The stator core losses are mainly made of the eddy current losses and the hysteresis losses. The eddy current losses can be calculated to

$$\Delta P_{eFe} = \frac{\pi^2 \sigma}{6} f^2 d^2 m_{Fe} [B_{mx1}^2 + B_{mz1}^2] \eta_d^2 \quad (2.49)$$

where d is the conductor diameter, m_{Fe} is the stator conductors mass, B_{mx1} and B_{mz1} are the magnetic flux density peak tangential and axial components respectively, and η_d is the coefficient of distortion. η_d is calculated by

$$\eta_d = \sqrt{1 + \frac{(3B_{mx3})^2 + (3B_{mz3})^2}{B_{mx1}^2 + B_{mz1}^2} + \dots} \quad (2.50)$$

where the eddy current losses in Eq. 2.49 is expressed under sinusoidal magnetic flux density if $\eta_d = 1$. The hysteresis losses are expressed using Richter's formula

$$\Delta P_{hFe} = \epsilon \frac{f}{100} m_{Fe} [B_{mx1}^2 + B_{mz1}^2] \eta_d^2 \quad (2.51)$$

where ϵ is a constant dependent on the material.

The PM losses that is most important is only applicable for machines with slotted stator ferromagnetic cores. The frequency of the magnetic flux density is

$$f_{sl} = s_1 p n. \quad (2.52)$$

The magnetic flux density that is due to the slot opening is expressed by

$$B_{sl} = a_{sl} \beta_{sl} k_C B_{avg} \quad (2.53)$$

where B_{avg} is from Eq. 2.37, k_C is from Eq. 2.26, and

$$a_{sl} = \frac{4}{\pi} \left(0.5 + \frac{\Gamma^2}{0.78 - 2\Gamma^2} \right) \sin(1.3\pi\Gamma) \quad (2.54)$$

$$\beta_{sl} = 0.5 \left(1 - \frac{1}{\sqrt{1+K^2}} \right) \quad (2.55)$$

$$\Gamma = \frac{b_{14}}{t_1} \quad K = \frac{b_{14}}{g'} \quad (2.56)$$

where $g' = g + h_M/\mu_{rrec}$, h_M is the magnetic thickness and μ_{rrec} is the magnetic permeability. The following variables are used to calculate losses generated by the PMs exited magnetic field

$$\beta_\nu = \nu \frac{\pi}{\tau} \quad (2.57)$$

$$\alpha_\nu = \sqrt{j\omega_\nu \mu_0 \mu_r \sigma} = (1+j)k_{nu} \quad (2.58)$$

$$k_{nu} = \sqrt{\frac{\omega_\nu \mu_0 \mu_r \sigma}{2}} \quad (2.59)$$

$$a_{R\nu} = \frac{1}{\sqrt{2}} \sqrt{\sqrt{4 + \left(\frac{\beta_\nu}{k_\nu}\right)^4} + \left(\frac{\beta_\nu}{k_\nu}\right)^2} \quad (2.60)$$

$$a_{X\nu} = \frac{1}{\sqrt{2}} \sqrt{\sqrt{4 + \left(\frac{\beta_\nu}{k_\nu}\right)^4} - \left(\frac{\beta_\nu}{k_\nu}\right)^2} \quad (2.61)$$

where σ is the electric conductivity and μ_r is the relative magnetic permeability. Assuming $\mu_{rrec} \approx 1$ the losses can be expressed as

$$\Delta P_{PM} = \frac{1}{2} a_{R\nu} k_z \frac{|\alpha|^2}{\beta^2} \left(\frac{B_{sl}}{\mu_0 \mu_{rrec}} \right)^2 \frac{k}{\sigma_{PM}} S_{PM} \quad (2.62)$$

where σ_{PM} is the electric conductivity, $\nu = 1$ and $\tau = 0.5t_1$ is assumed. To calculate the reactive losses exchange $a_{R\nu}$ with $a_{X\nu}$. The coefficient k_z is calculated by

$$k_z = 1 + \frac{t_1}{D_{out} - D_{in}} \quad (2.63)$$

where D is the PM diameter. The surface area of all PMs is

$$S_{PM} = \alpha_i \frac{\pi}{4} (D_{out}^2 - D_{in}^2). \quad (2.64)$$

The losses of the rotor is calculated similarly to the PM losses but the coefficients $a_{R\nu}$ and $a_{X\nu}$ are replaced with

$$a_{RFe} = \frac{1}{\sqrt{2}} \left[\sqrt{4a_R^2 a_X^2 + \left(a_R^2 - a_X^2 + \frac{\beta^2}{k^2} \right)^2} + a_R^2 - a_X^2 + \frac{\beta^2}{k^2} \right]^{\frac{1}{2}} \quad (2.65)$$

$$a_{XFe} = \frac{1}{\sqrt{2}} \left[\sqrt{4a_R^2 a_X^2 + \left(a_R^2 - a_X^2 + \frac{\beta^2}{k^2} \right)^2} - a_R^2 + a_X^2 - \frac{\beta^2}{k^2} \right]^{\frac{1}{2}} \quad (2.66)$$

where $a_R = 1.3$ to 1.4 , $a_X = 0.8$ to 0.9 , k is from Eq. 2.59 and β is from Eq. 2.57 for $\nu = 1$.

The rotor losses can then be expressed as

$$\Delta P_{Fe} = \frac{1}{2} a_{RFe} k_z \frac{|\alpha|^2}{\beta^2} \left(\frac{B_{sl}}{\mu_0 \mu_r} \right)^2 \frac{k}{\sigma_{Fe}} S_{Fe} \quad (2.67)$$

where most variables are the same as Eq. 2.62. Same as for Eq. 2.62 the reactive losses are calculated by replacing a_{RFe} to a_{XFe} . The surface of the rotor disc is

$$S_{Fe} = \frac{\pi}{4} (D_{out}^2 - D_{in}^2). \quad (2.68)$$

The eddy current losses in the stator windings are ignored for slotted machines but otherwise is calculated for round conductors by

$$\Delta P_e = \frac{\pi^2}{4} \frac{\sigma}{\rho} f^2 d^2 m_{con} [B_{mx1}^2 + B_{mz1}^2] \eta_d^2 \quad (2.69)$$

2.4.7 Power System

The power system for the generator and load can be simplified to a single circuit diagram and phasor diagram which enables easier calculations and makes the diagrams the same independent on the number of phases. The circuit diagram equivalent for a star connected generator, see figure 2.3, by [23] gives the equation for the system as

$$E_f = V + I(R_s + jX_s) \quad (2.70)$$

where V is the line voltage for one phase, I is current through one phase, R_s and X_s are stator resistance and reactance respectively. The terminal voltage for star connection is $V_t = \sqrt{3}V$ while the line current is the same as the terminal current. Using the equations gives the phasor diagram in figure 2.4, where δ is the angel

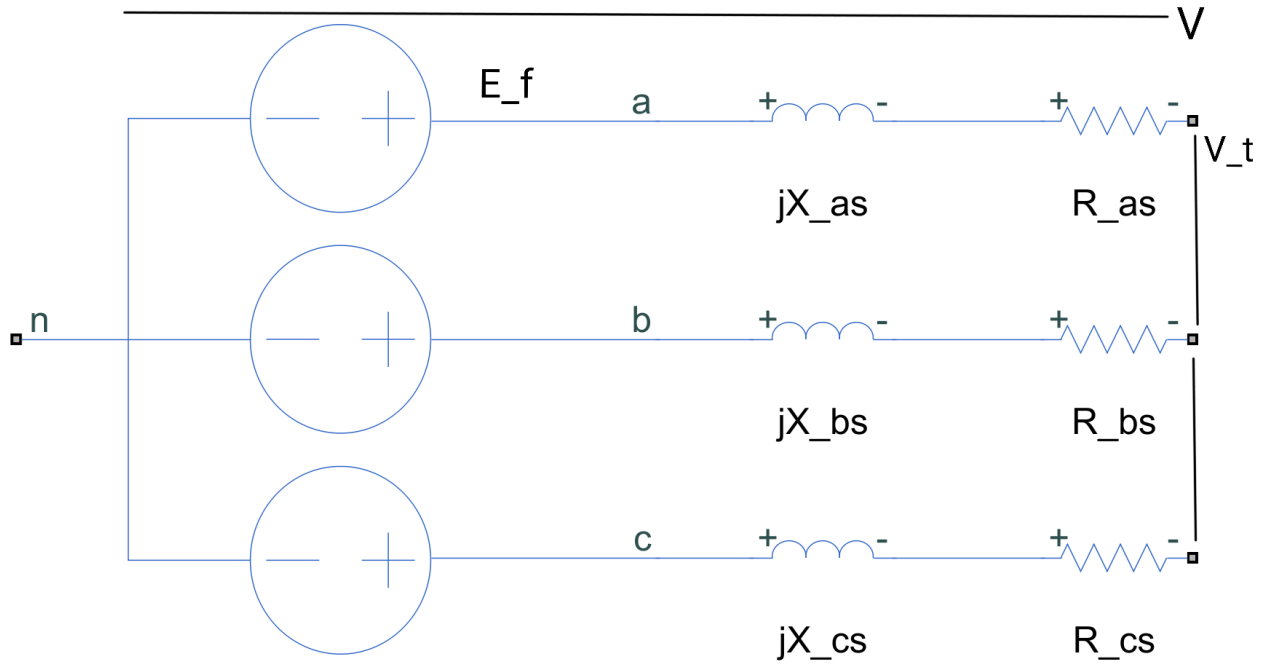


Figure 2.3: Star connected three phase diagram.

between the voltages θ is the angle between the terminal voltage and the current. The terminal voltage can be expressed using the current and load as

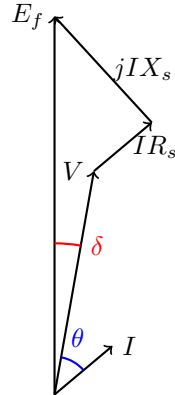


Figure 2.4: Phasor diagram.

$$V = I \sqrt{R_l^2 + X_l^2} \quad (2.71)$$

where R_l and X_l are the load resistance and reactance respectively. Using the new expression in the phasor diagram, see figure 2.5, results in the expression

$$E_f = I \sqrt{(R_s + R_l)^2 + (X_s + X_l)^2} \quad (2.72)$$

and

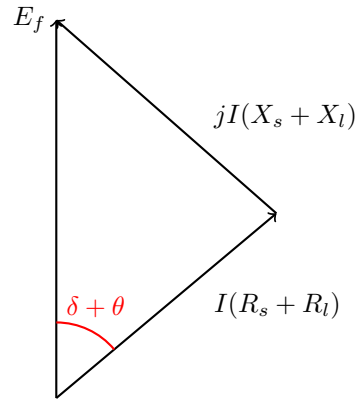


Figure 2.5: Phasor diagram with the load impedance.

$$\delta + \theta = \arctan \frac{X_s + X_l}{R_s + R_l}. \quad (2.73)$$

The power for one phase from the generator is expressed as

$$P_{phase} = VI \cos \theta = \frac{E_f V_t}{\sqrt{(R_s + R_l)^2 + (X_s + X_l)^2}} \cos \theta \quad (2.74)$$

and for three phases

$$P = 3P_{phase}. \quad (2.75)$$

Chapter 3

Requirements

The requirements for the hydropower system are based on the idea of a small and easy to install system. The requirements for the system, which can be tested and evaluated, are not so many, see table 3.1. The reason why not more requirements are needed is because it only has a single variable input, water flow, and its output can easily be converted to any desired system if the minimum output is reached. There are however other restrictions on the system that while not required needs to be considered. The primary restriction is the possibility to construct the system for testing. This can restrict on certain material used or not being able to manufacture the optimal part for the system. A second restriction is to simplify the design if possible since then its more likely to be reliable and easier to construct. Reliability or simplicity of design is not evaluated but is always good to consider when developing since the design could lead to a finished product.

3.1 Requirement of the Generator

The generator has few requirements on it specifically but are limited in its construction capability. The limiting factors from the requirements is its width and output power rating. There is no specific limitation on the length of the generator, but it is desired to be as compact as possible. The width requirement does have restrictions on the number of magnetic pairs and coils. The output requirement is independent on the number of phases since a converter circuit can turn the AC to DC with low losses. For similar reasons the voltage and current values can be altered to fit any need if the minimum power is achieved. However, it is desired to have a low current compared to voltage and the design should have that in consideration.

3.2 Requirement of the Turbine

The turbine part is required to fit inside a small water pipe which limits its dimensions. The turbine part length is restricted to the pipe diameter and can't exceed the maximum length therefore the turbine must be slightly shorter than the housing around it. The width of the system, and therefore also the turbine part, is limited. The

limitation is to enable installation in existing pipe system, where the hydropower system is installed from the outside through a hole. This also limits the turbine further as it needs to be smaller than the systems housing, same as its length. The requirements on the outer dimensions limits the turbine to a vertical axis system for maximal cross-sectional area coverage.

Table 3.1: Specification for the hydropower system

Turbine Part Max Length	50	mm
System Max Width	10	mm
Min Power Rating	1	mW
Max Water Flow	10	m/s

Chapter 4

Analysis and Design

For designing the energy harvester, two different types of turbine were tested using the same generator design. The different designs were a reaction and an impulse turbine type. Both designs shared many similarities between them, both are a vertical axis turbine with the same type of central axis and overall dimension. The impulse turbine is a more classical approach of the two while the reaction turbine is based more on wind turbine design. The impulse turbine design is based on the Pelton wheel, in such way that the water's kinetics energy drives it rather than the reaction type which redirects water which creates pressure differences. The common way to implement a water turbine in pipes is to use a bypass which enables one to direct the water the desired way for the specific turbine. As the desired energy harvester should be a small compact package which can be installed without modifying the pipe to construct bypasses forces the device itself to direct the water flow in the desired direction.

4.1 Impulse Turbine Design

The Pelton wheel can not work as it is underwater as well as designed without redirecting the water flow into a concentrated area on the turbine. This can be achieved by having an outer wall, blocking part of the turbine from the incoming water flow. This outer wall will also be the main supporting structure for the turbine. The turbine blades are designed to catch as much water as possible and have a bucket shape to them, see figure 4.1, with baffles on the bottom part as can be seen in figure 4.2. As is shown by [10], the optimal number of blades on the turbine is five.

4.2 Reaction Turbine Design

The reaction turbine design is based on the vertical axis wind turbine design because of the similarities between how torque is generated. The difference comes from the different medium, i.e. fluid compared to air, but the main principle is the same with lift/drag forcing the rotation. Its advantage, and also disadvantage, is that it

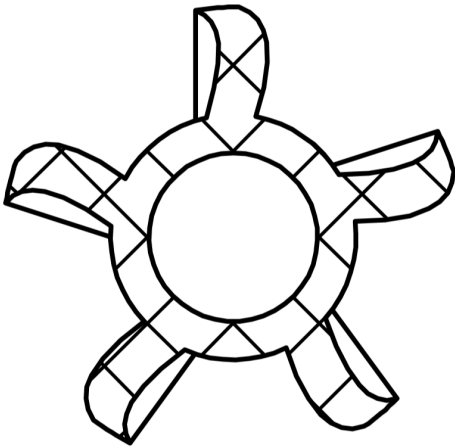


Figure 4.1: Impulse turbine blades top view.

can generate torque independent on the incoming fluid direction. The disadvantage when flow only comes from one direction is a loss in efficiency compared to turbines design around flow from a single direction. However, the flow does not need to be controlled because of its advantage, compared to the impulse design, enabling larger volumes of fluid through it. The blade design is based on an airfoil, NACA 0015 see figure 4.3, however its small size forces some design aspect to differ from the optimal to enable construction, see figure 4.4 for the modified version. This alteration will reduce the lift/drag force of the blade from the given data, see figures 4.6. Another factor which needs to be considered is the low Reynolds number derived from its small width, $Re < 5000$, resulting in the true lift/drag values lower than those portrayed. To ensure a smoother torque curve, and therefore more consistence power generation, the blades was twisted in a helical design, rather than straight. For the optimal stability as express by [24], three blades were chosen where the blades are symmetrical, see figure 4.5, and to increase power the blades were angled at $\beta = -4^\circ$.

4.3 Generator Design

The requirement of the energy harvester demands high energy efficiency to size which makes the axial flux permanent magnet (AFPM) generator the best option. The design will be divided into the stator and rotor part as there are many different ways to construct a AFPM generator. A large focus on the design will be on the possibility to physically construct it without excessively expensive parts. To have the highest efficiency for the generator the Halbach array is used for the PMs arrangement, which gives the lowest number of pole pares to $p = 4$. Because of the limited minimum size for PM available the highest pole pair possible was $p = 4$. The size of the PMs is a cube of width 1mm of material $NdFeB$, with magnetisation $N45$. The magnetic flux density in the z direction is $0.47T$ but the flux density in x direction can not be calculated without simulation and can therefore be assumed to be the same as in the z direction when calculating losses.

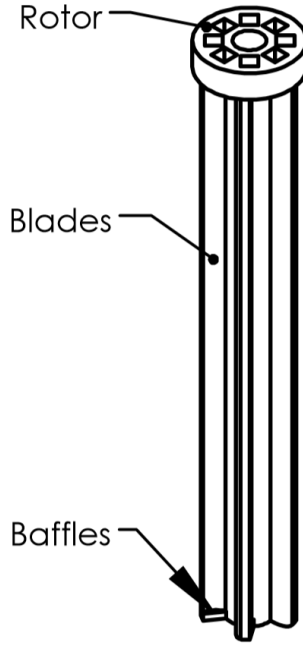


Figure 4.2: Impulse turbine.

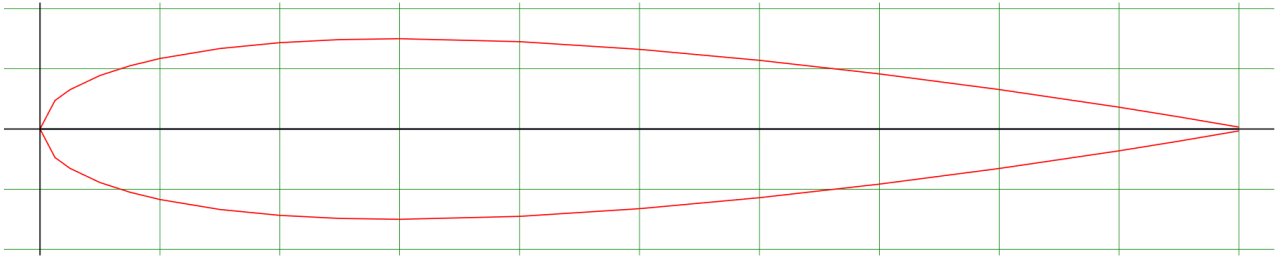


Figure 4.3: Airfoil NACA 0015 shape.

The generator was chosen to be core-less in both the rotor and stator because of the small scale of the generator together with the necessity to construct it by hand. This does not cause a large problem since PMs have a high flux density and AFPM have a high efficiency. The rotor and core losses also disappear, leaving only the eddy current losses of the coil windings left which are ignored in a slotted generator. To maximise the possible density of coils in the stator while still being able to wound them by hand is found to be $s = 6$. A three-phase generator setup was chosen to increase the winding factor despite the increased difficulty in testing its output without a oscilloscope. One way around this problem is to only measure one phase and then use its symmetry to calculate the total output. Using the equations 2.28-2.31 gives the winding setup with coil groups $z = 1$ and the number of coils per phase to $n_c = 1$. The winding factor can be calculated using the values from table 4.1 to $k_{wi} = 0.8660$ for iron cored and $k_{wa} = 0.8588$ for air cored. Because the winding factors are almost the same, air cored windings were chosen as they are easier to make. The wire used for the coils is an emailed copper wire of thickness $0.1mm$. The values of the coils and stator side is found in table 4.1. To

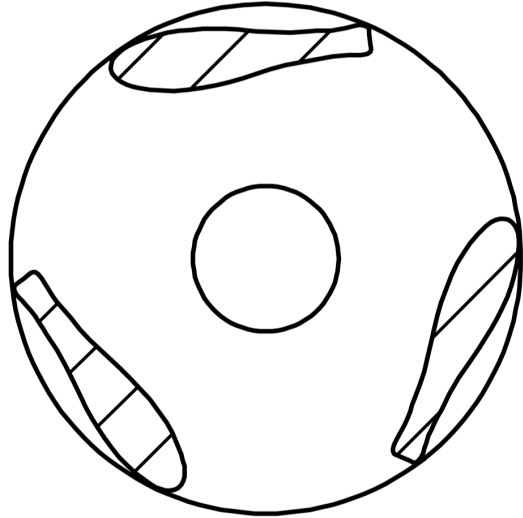


Figure 4.4: Reaction turbine blades top view.

calculate the optimal load for the system the power equation 2.74 were used for a set value of RPM with load as a variable, see figure 4.8, where $R_l = 3$ is optimal. The load was chosen as only a resistance since adding reactance would have low impact since $R_L \gg X_L$ even at high RPM values.

Table 4.1: Stator coil variables

r_{in}	0.8mm
r_{out}	2.2mm
d_{wire}	0.1mm
N	35
R_{coil}	3.68Ω
L_{coil}	$64\mu H$
z	1
s	6
m	3

4.4 Complete Construction

The turbines are supported by a outer structure which serves both as the connection point between the central axis and the turbine as well as the stator part of the generator, see figures 4.10-4.9. The rotor part of the generator is connected directly to the rotor, as is shown in figure 4.2 and 4.5, in a way to simplify the design. The connections enable the central axis to only be connected to the turbine and the outer support structure, reducing weight and simplifies waterproofing. The turbine is connected to a central rod which in turn is connected to two ball bearings on the support structure, only the lower bearing is seen in figures 4.10-4.9 while the other is above the stator. The top part of the outer structure is open which enables ease of access to the central axis, enabling fast dismantling of the turbine and access to the rotor and stator. During testing leakage can occur between the central axis and the upper ball bearing but that problem could easily be fixed by sealing the top part of.

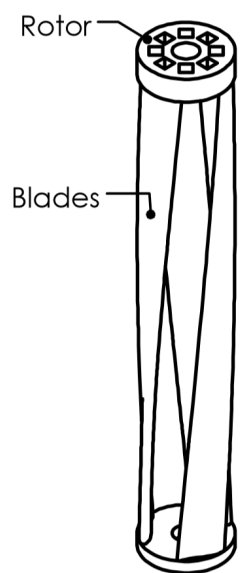


Figure 4.5: Reaction turbine.

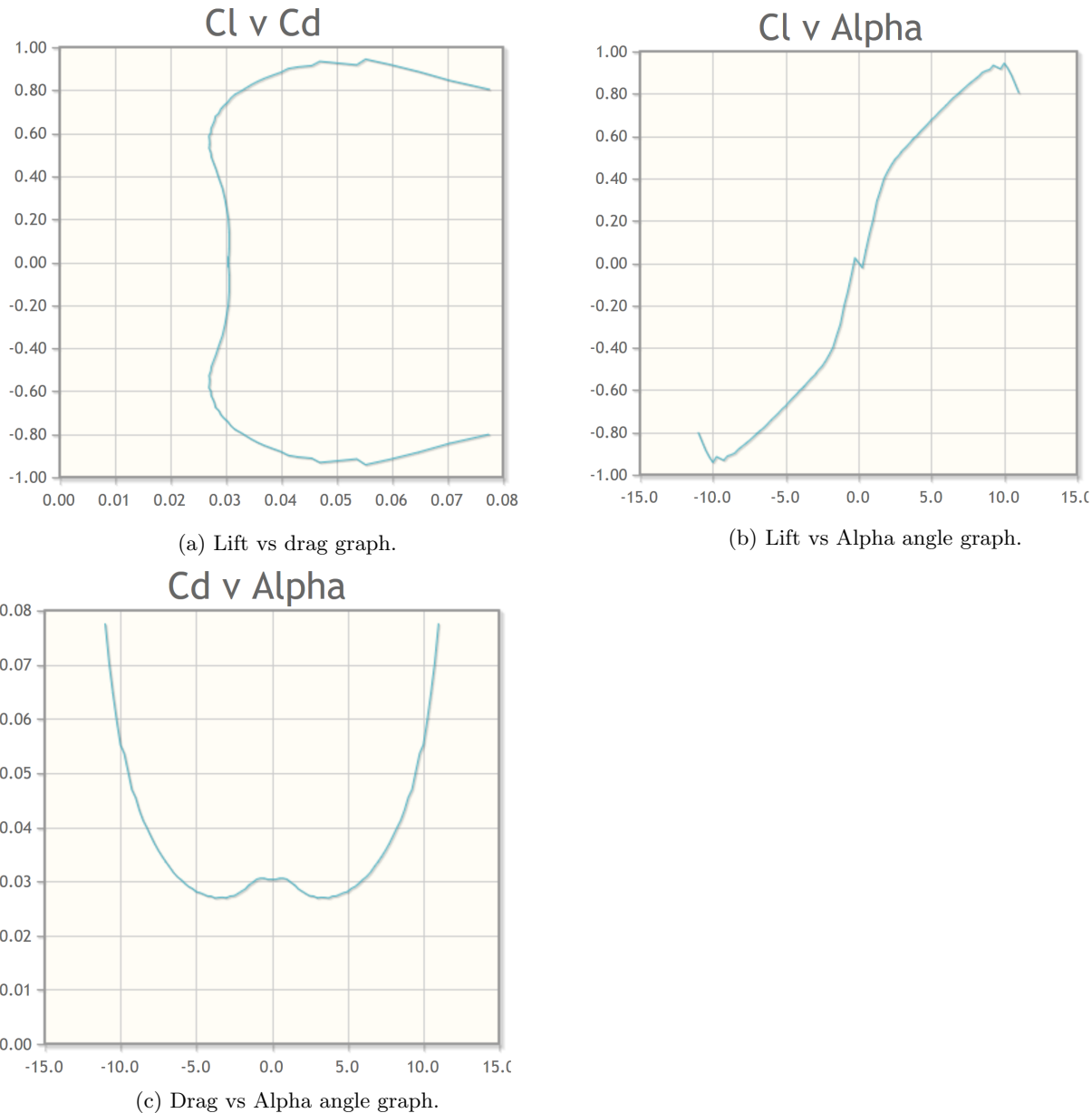


Figure 4.6: Lift and drag graphs for airfoil NACA 0015 at Reynolds number $Re = 50000$.

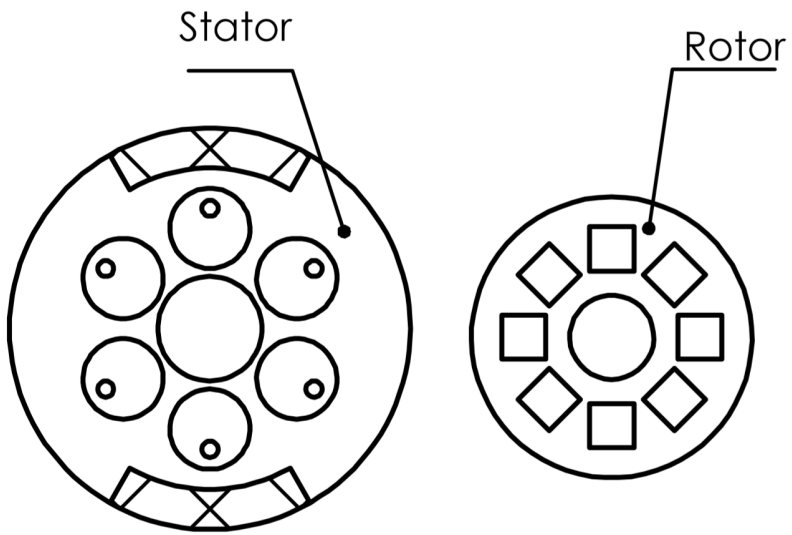


Figure 4.7: Generator view.

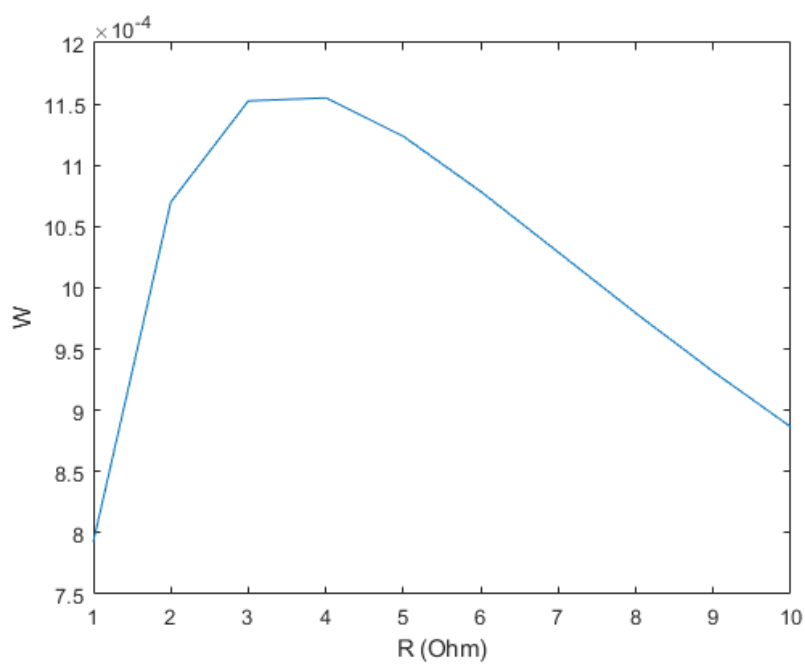


Figure 4.8: Power as a function of load at 30000 RPM.

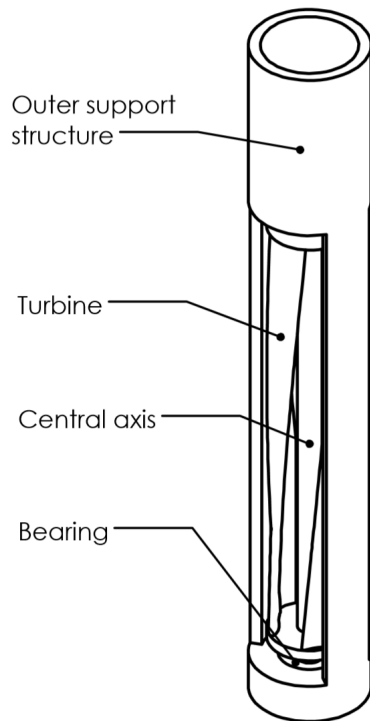


Figure 4.9: Reaction turbine design.

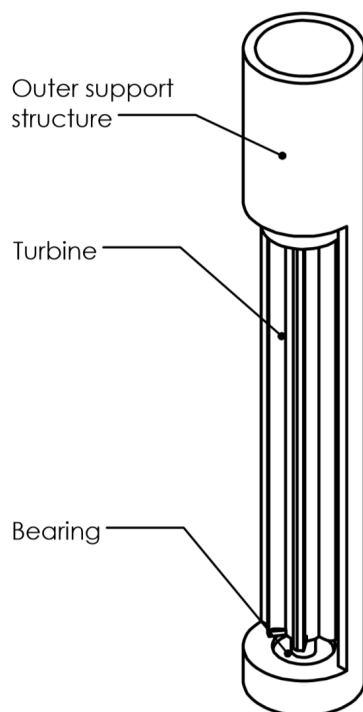


Figure 4.10: Impulse turbine design.

Chapter 5

Implementation

The methodology used to calculate the different variables for the turbines and generator is explained through flowchart or simulations meant to easily be understood and utilised rather than specific code segment. The necessary equations used to get the variables can be found in chapter 2. The construction method used and reasoning behind the chosen decision is explained together with figures showing the parts in detail enable a comprehensive understanding of the structure.

5.1 Designing

The impulse turbine design is based on the one used by [10] and the shape can be seen in figure 4.1. The power interacting on the turbine is shown in figure 5.1, but the efficiency can not be estimated as the necessary simulation software is lacking. Its efficiency will therefore be measured through the testing of the turbine.

The reactive turbines design and generated power can be calculated using MATLAB by following the procedure by [12] shown in the flowchart in figure 5.2. Using the procedure to get the induction factor a the power coefficient can be calculated for the different values of TSR using equations 2.11-2.23 as can be seen in figure 5.3. The airfoil used gives the drag and lift curves needed to calculate the coefficients, see figure 4.6. The efficiency graph shows that the turbines require a high TSR to work at its max capacity. While its unlikely that it operates at those TSR values, assume a TSR of $\lambda = 2$ gives the values found in figures 5.4.

The values and parameters for the axial flux PMSG is calculated in MATLAB following the flowchart logic in figure 5.5. Using the flowchart gets the generator values and then the set load needs to be calculated to reach optimal value. The necessary equations for all calculation is found in chapter 2.4. Using the values from section 4.3 gives the calculated power values in figures 5.6.

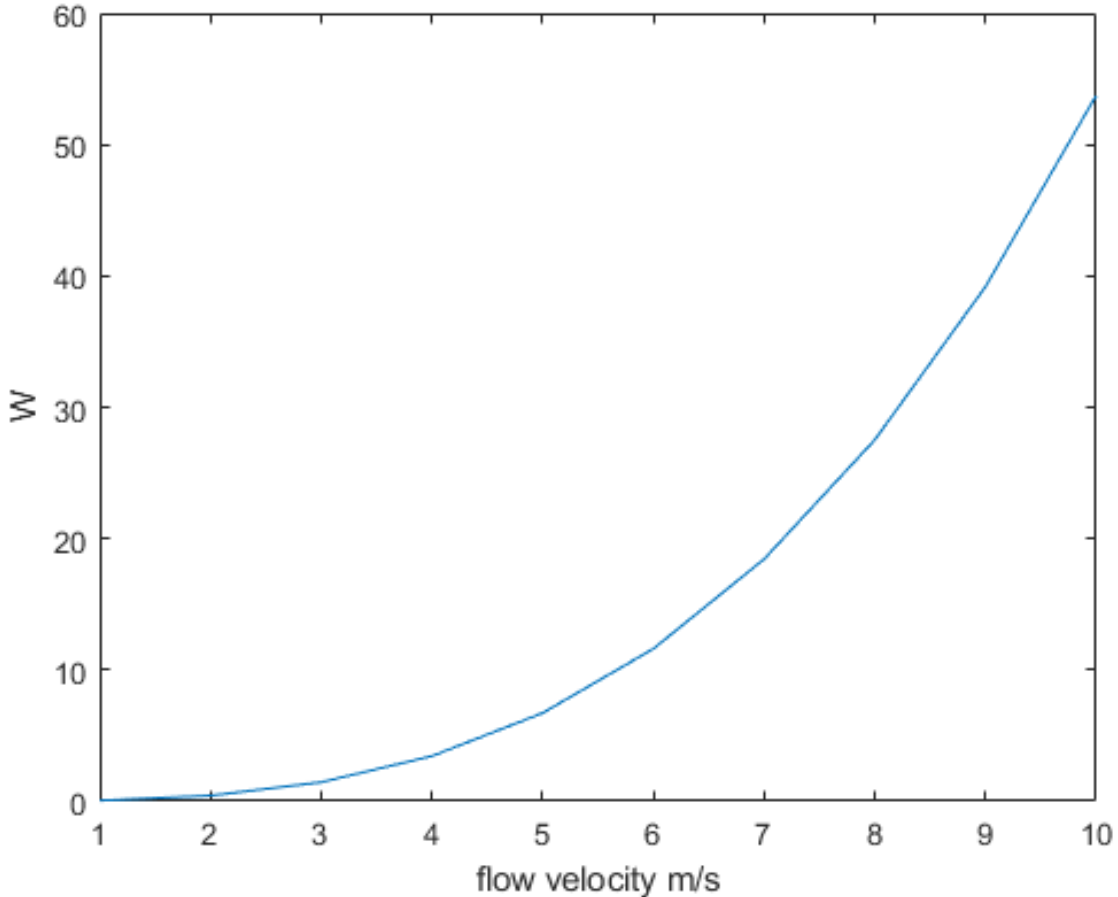


Figure 5.1: Power from flow interacting on the impulse turbine.

5.2 Constructing

The designing of the turbine parts together with the outer support structure is done in SOLIDWORKS as a 3d model. The usage of a 3d model enabled precise details on small scales which would not be easily or cheaply replicated. The parts were 3d printed in plastic variant material, the reaction turbine was printed in Objet™ 'Polymerjet' Resin while the impulse turbine was printed in PLA (Polylactic Acid) material, because of the fast production time and cheap cost. The disadvantages with the plastic material are structural strength and flexibility, but for a prototype design the durability is less interesting as long as the design holds for the duration of the tests. The reason for the different material used was that different suppliers produced the different turbines, the first supplier could not make the second design because of COVID-19 and another supplier was therefore approached. The support structure schematic for the impulse turbine design is shown in figure 4.2 and for the reaction turbine in figure 4.5. To see more detailed schematic of the parts see appendix A.

The coils for the stator was hand wound around a metal wire of thickness 0.7mm. The exact number of turns for the coils was tested using the restriction of fitting in the designed space, see figure 4.7, since a higher number would result in higher voltage values, which resulted in 35 turns. The coils were glued to keep it in the

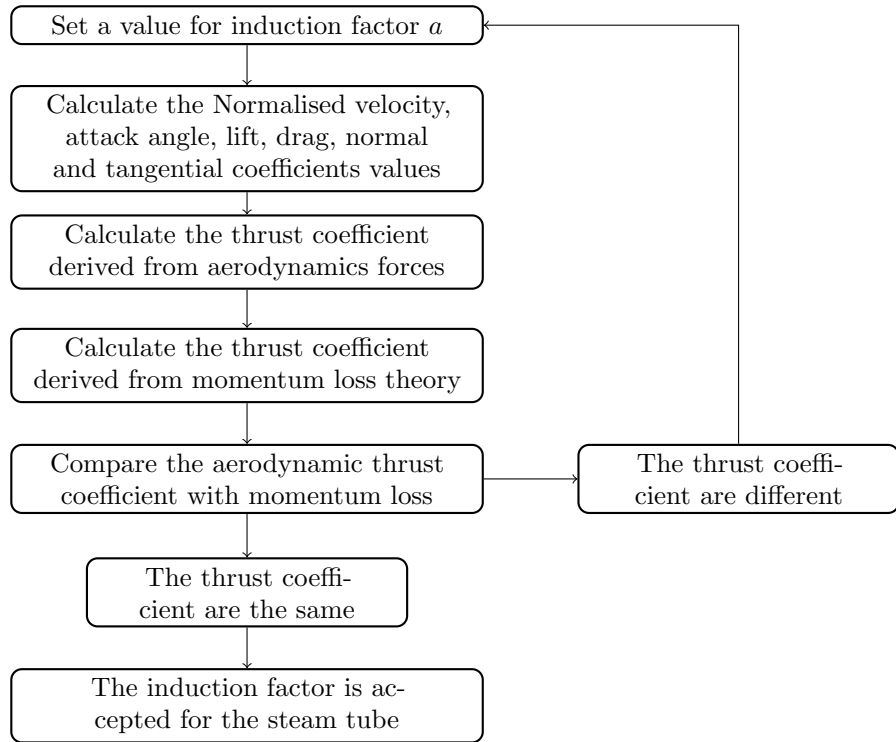


Figure 5.2: Iterative flowchart to calculate the flow velocity.

desired shape and have the air core after removal form the metal wire it was wound around. The end connections from the coils were then pushed through the small hole located in the slots to enable easier connection and remove the wire form the water. This worked for the reaction turbine design but not for the impulse design. The 3d printer used by the supplier was not precise enough to make holes of that diameter which resulted in the wire connections needed to be brought on the outside of the structure.

The PMs for the rotor was inserted on the top of the turbines in designed slots, see figures 4.7, in a Halbach array. Similarly, as before, the slots also suffered from the second 3d suppliers in that the slots could not fit the PMs. Therefore, a spare part from the reaction turbine was used as the rotor, connected to the top of the impulse turbine. The turbine itself was connected to a stainless-steel axis, see figures 4.9-4.10, acting as support and connecting the turbine to the support structure. The axis was inserted from the top and was connected to two steel ball bearings, located in the lower inside and in the top part of the support structure. The insertion of the turbine from the side and the axis from the top enables ease of removal and access to all different parts.

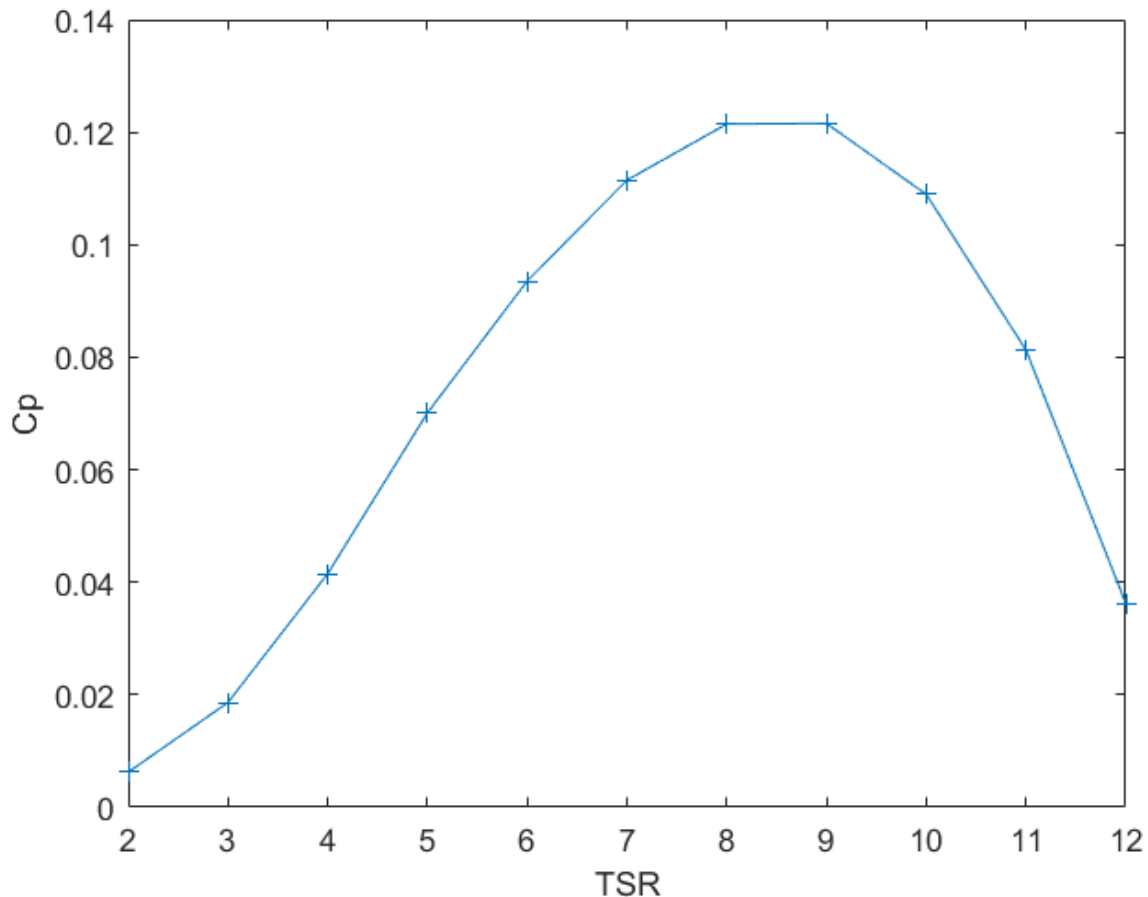
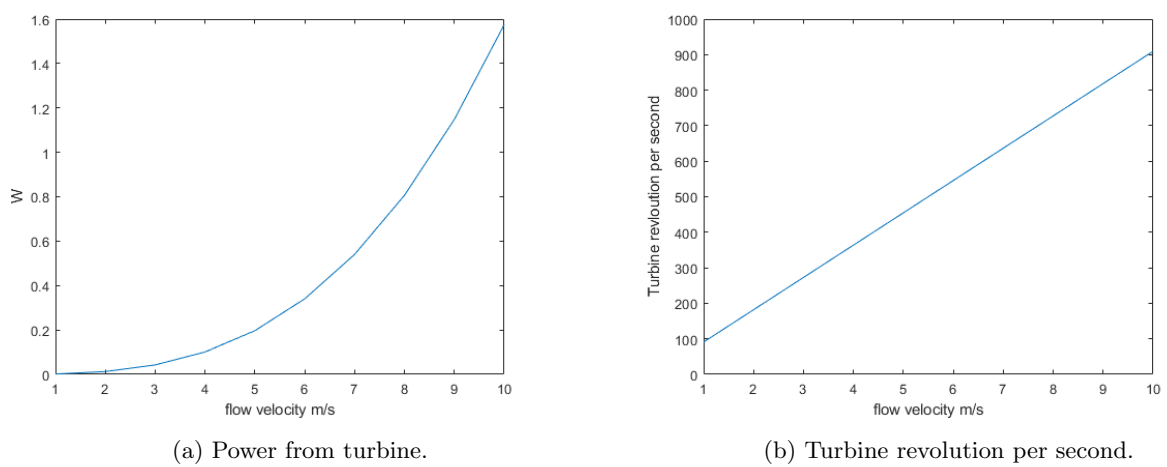


Figure 5.3: Graph of power coefficient based on TSR.

Figure 5.4: Graphs of reaction turbines output values at $\lambda = 2$.

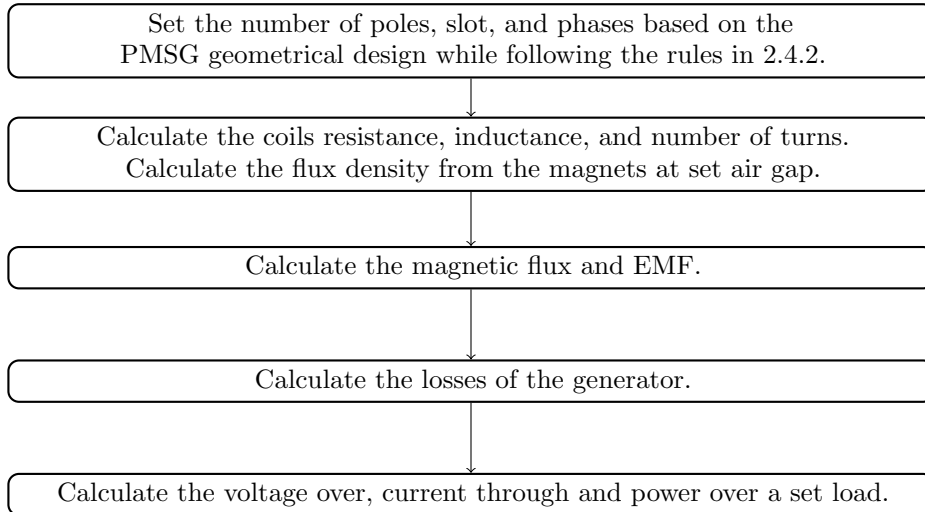
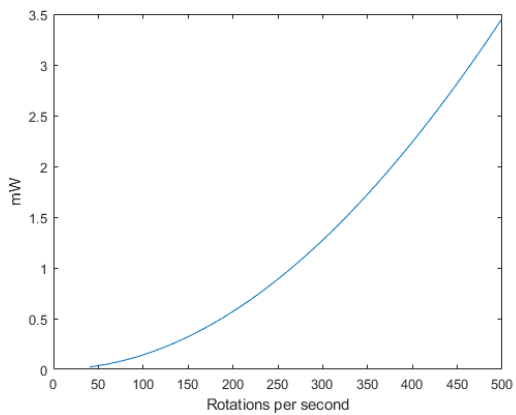
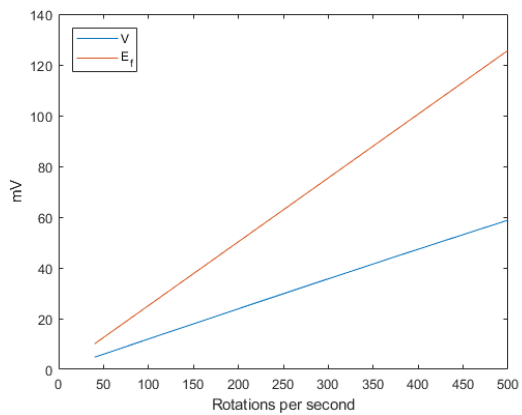


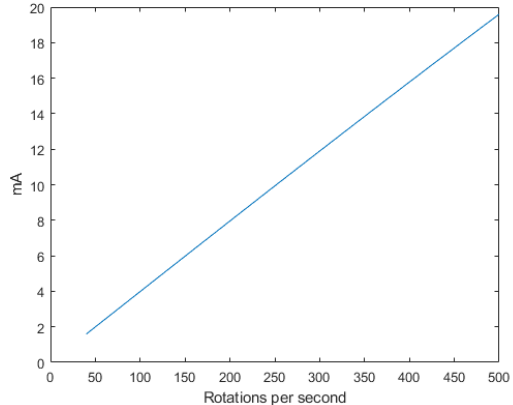
Figure 5.5: Iterative flowchart to calculate the values of the axial flux PMSG.



(a) Total Power from generator.



(b) EMF and voltage over load from generator.



(c) Current through load from generator.

Figure 5.6: Graphs of output values at tangential velocity matches flow velocity.

Chapter 6

Testing

To test the hydropower turbine a costume water test rig was constructed, a more advanced water testing rig was not available because of COVID-19 outbreak. The test was run on different flow rates where the current and voltage was measured using a multimeter.

6.1 Testing Rig

The testing rig consisted of a variable speed water pump, see table 6.1 for specification together with figure 6.1, connected to a closed loop pipe system. The pipe system was constructed of $50mm$ diameter PVC pipe in a tight loop around the pump, see figure 6.2. To insert the hydropower turbine a $12mm$ hole was drilled into the topmost part of the pipe where the hydropower turbine could be inserted. Because of the slight dimensional miss match between the hydropower turbine, which was $50mm$ long, and the pipe which outer diameter also was $50mm$, some leaking occurred which was mostly mitigated with the application of duct tape. Another slight problem was the existence of air pockets inside the closed loop which could not be removed because of the pumps structural design. For the testing of the hydropower turbine the water flow had to be guessed based on the set RPM on the water pump against the flow chart in figure 6.1 which makes a precise flow hard to establish.

Table 6.1: Water Pump Specification

Name	Zodiac FloPro VS
Motor Power	$1.2kW$
Pipe outer diameter	$50mm$
Pipe inner diameter	$46.3mm$
Operation range	$600 - 3450RPM$
Maximum pump flow	$30.7m^3/h$

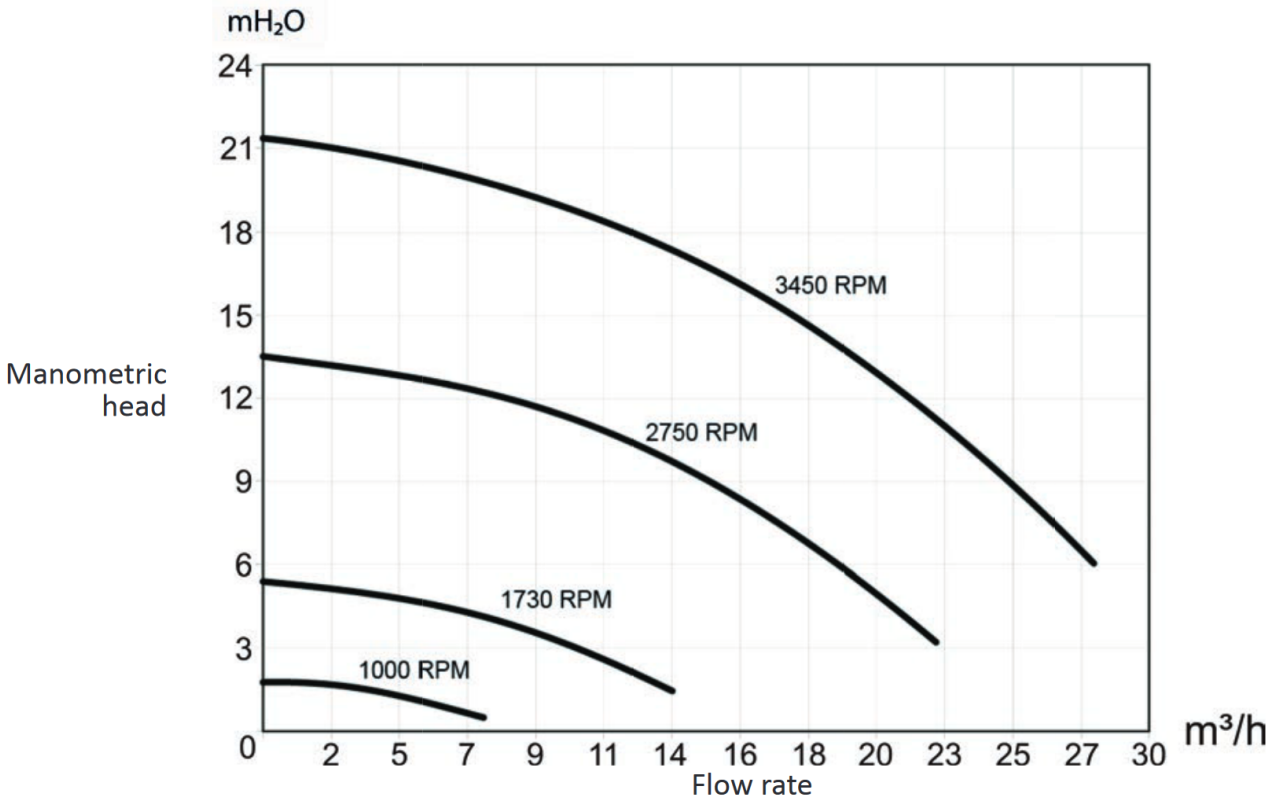


Figure 6.1: Water Pump Flow Chart

6.2 Method

The testing of the different designs is implemented by inserting the hydropower turbine into a hole drilled through the pipe, see figure 6.3, and restricted through duct tape. The usage of duct tape ensured a compact seal, reducing the water leakages, while also being easily removed. The hydropower turbine is rotated around its z-axis to ensure maximal torque to the turbine by changing the amount of flow blocked by the support structure. The testing of the device, measurement of voltage and current, was done for different water flow velocities which was regulated by the change of pump RPM. The different flow velocities that the device will be tested in is shown in table 6.2. The highest pump RPM used for the testing is lower than its maximum because of the high forces on the test rig, making it unstable to test on. For each RPM values of the pump the hydropower turbine open voltages as well as voltage over and current through load was measured and compared to the calculated values. From the measurements the power generated over the load and its efficiency can be established and compared to the desired outcome.

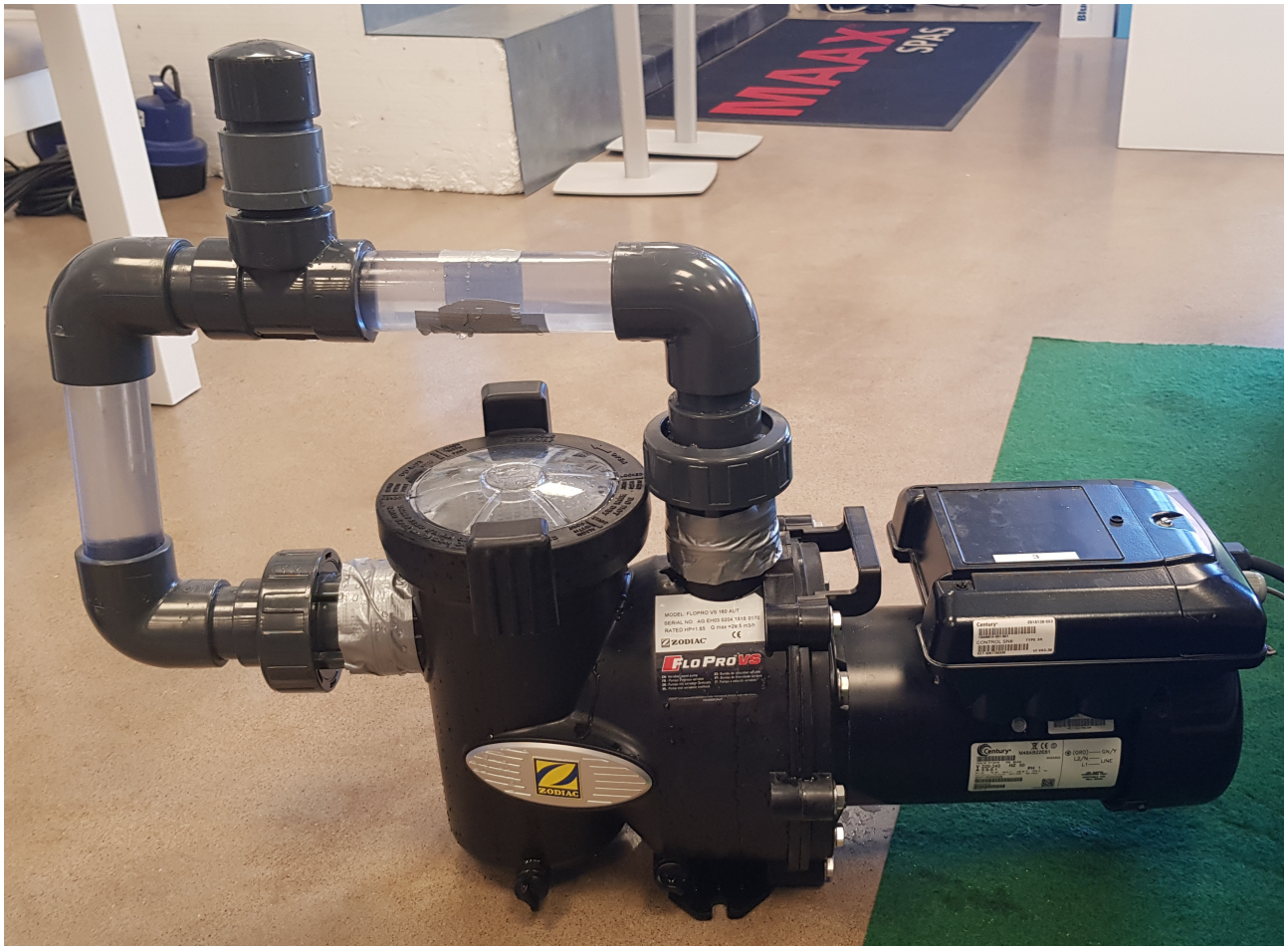


Figure 6.2: Flow Rig

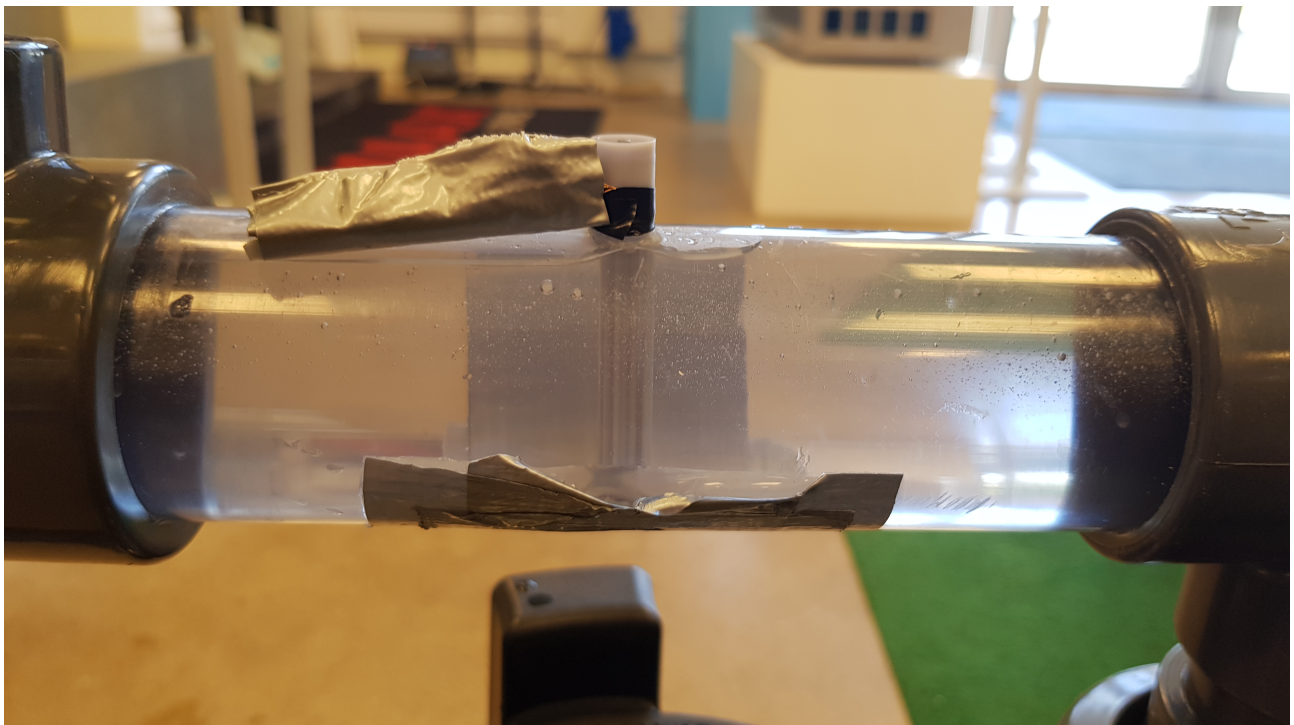


Figure 6.3: Inserted hydropower turbine

Table 6.2: The water flows are based on figure 6.1 and not a formula or measurement. Therefore the exact flow values may differ from the ones in the table.

Pump RPM	Water Flow
800	$0.9m/s$
1000	$1.1m/s$
1300	$1.6m/s$
1700	$2.2m/s$
2300	$3.0m/s$
2900	$4.0m/s$

Chapter 7

Results

7.1 Impulse Turbine Results

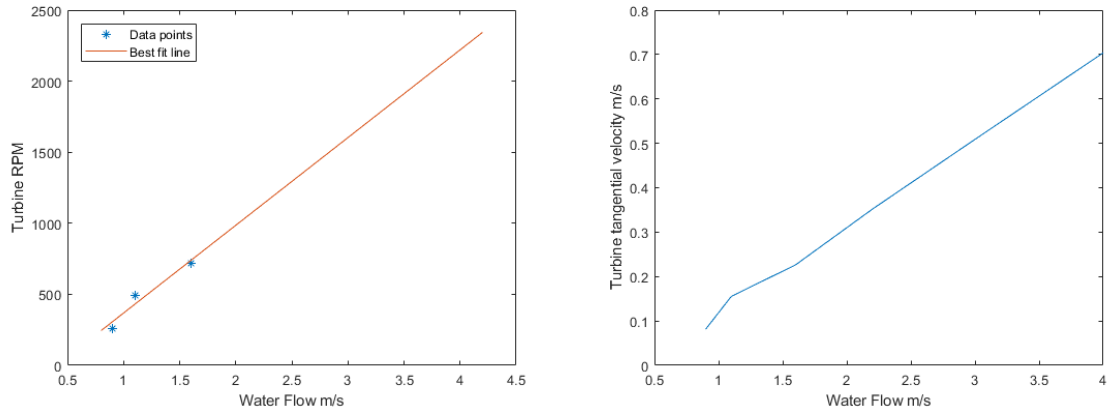
The testing of the impulse turbine design in the test rig showed that it successfully rotated at all tested flow velocities however the generator failed to produce any measurable results for all tests. Because of this failure to either measure or more likely produce any power from the generator the turbines performance could not be measured, resulting in a lack of testing data. The only results captured was video of the turbine for each flow velocity. Using the video, the turbines RPM could be calculated for the lower flow velocities, see table 7.1. Using the calculated turbine RPM for the low flow values and then assuming a linear relationship between the water flow and the turbine RPM results in the graph in figure 7.1a. The turbines power can then be calculated using its RPM value together with the equations 2.6-2.10, see table 7.2, as well as its tangential velocity, see figure 7.1b. The turbine is found to be most efficient when angled -15° , see figure 7.2, resulting in a large part of the turbine blocked from the flow.

Table 7.1: The turbine RPM calculated for video footage.

Pump RPM	Water flow	Turbine RPM
800	$0.9m/s$	260
1000	$1.1m/s$	495
1300	$1.6m/s$	720

Table 7.2: The turbine power and efficiency calculated.

Water Flow	Turbine Power (Only flow through turbine)	Efficiency	Efficiency (Total)
$0.1m/s$	$0.5mW$	1.6%	0.3%
$1.1m/s$	$3.6mW$	5.8%	1.1%
$1.6m/s$	$11.3mW$	5.8%	1.1%
$2.2m/s$	$42.5mW$	8.5%	1.7%
$3.0m/s$	$128.6mW$	10.1%	2%
$4.0m/s$	$340mW$	11.3%	2.2%



(a) Best fit line of the impulse turbine RPM based on the data points.
(b) Turbine tangential velocity compared to flow velocity.

Figure 7.1: Impulse turbine results.

7.2 Reaction Turbine Results

The testing of the reaction turbine design in the test rig showed that the design failed to generate torque for any flow velocities. Because of the lack of rotation, the generator could not be tested which resulted in no testing values presented in the report. The turbine design failed to generate enough lift/drag to rotate, resulting in a failed design.

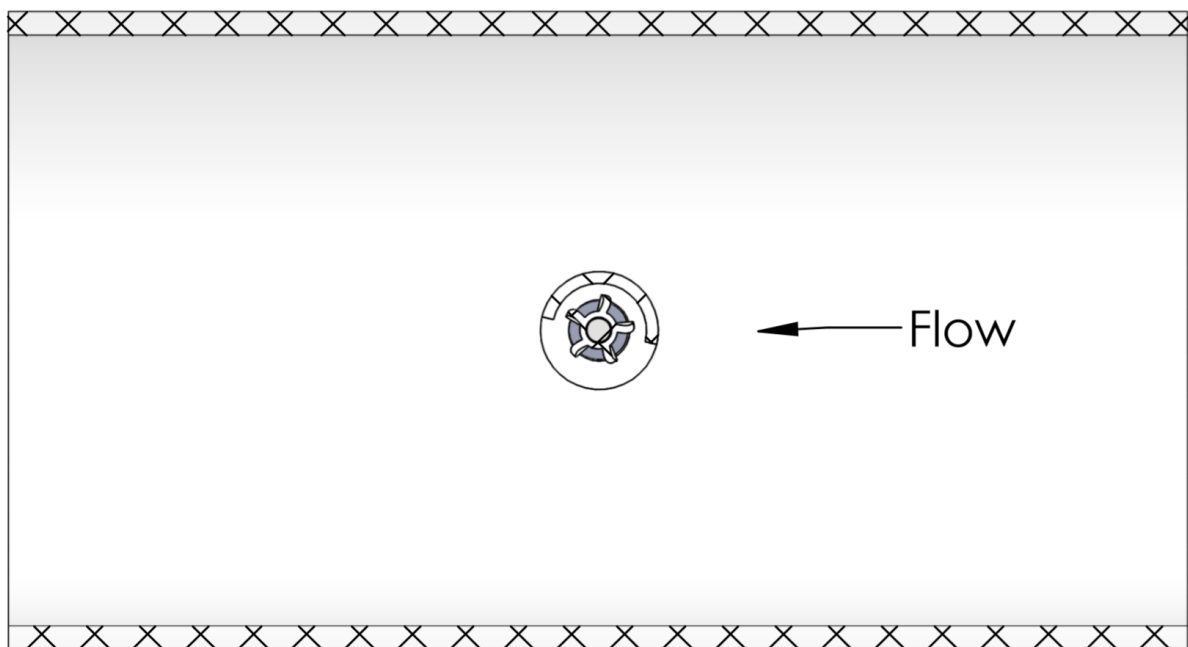


Figure 7.2: Impulse turbine connected in the pipe at a -15° angle.

Chapter 8

Conclusions and Further Work

8.1 Evaluation

The turbines themselves preformed below the expected values, with the reaction type not producing any torque. The impulse turbine did produce the required power as rotational energy for flow velocities of $< 1m/s$, excluding generator efficiency, but the low RPM fell far below the generators desired range. Its tangential velocity was only 1/10 of the water flow velocity when it would ideally match or exceed it. When taking the efficiency into consideration than only a few percentages of the power were converted, however when only consider the flow impacting the turbine blades its efficiency increases along higher flow rates. This efficiency difference can be expected as the impulse turbine design requires more controlled water direction than reactor types. This can easily be seen by comparing to other impulse turbine designs, such as the design by [10] whom forced the flow in a vortex around the turbine and drained it away at the bottom. Another impulse turbine design that doesn't have the same issue with directing the flow is the cross-flow turbine used by [25] which also have a vertical axis. The difference with them and most other is the scale of the turbine. The scale is also the large issue with reaction types as they reacquire lift/drag to rotate which is based on the Reynold number and as it's greatly reduced for small cord lengths. The reaction turbine was designed as a Darrieus water turbine as the more common one used, the Francis or Kaplan turbine, have a greater width than height which would result in a small flow area coverage. These types of turbine are more common as they have higher efficiency but require alterations to the pipe to operate as designed, such as the pipe inline Kaplan turbine used by [26] which reached an efficiency of 60%.

The generators results are difficult to comment on as the turbines didn't reach a reacquired RPM for it to operate efficiently and no equipment were available to test the generator separately. Some problem arouses surrounding the construction and printing of the generator, such as the issue of the coil connections not being able go through the back, but otherwise it's difficult to guess if the design would have worked. When compared to other designs of similar scale the biggest difference was the fabrication method. Both [27] and [7] uses machines to produce the components of the generator, giving a much higher precision for each part but also increases the

difficulty of production. However, none of those have been used together with a water turbine but they do have the same desired high RPM value. For the generators used on the water turbines they are always external radial generator with no constraint on size, and often not mentioned in detail, so any comparison is hard to make.

8.2 Turbine Conclusion

The turbines designed that were tested both worked less well than desired, with the reaction type not working at all. The reaction turbine design was based on vertical axis wind turbine design, and similarly under water design types, because it offered the desired vertical axis, with the width being more restricted than the height, while also having a solid axis. The reasoning behind the importance on the solid axis is the risk for structural damage without a hard support material as support. The small scale is the largest problem for the design of this type of reaction turbine and the reason why it didn't work as desired, both with the designing and manufacturing. The small scale of the blades resulted in a low Reynolds number, and low lift/drag force, which could not rotate the turbine. The helical rotation on the blades were an attempt to make the torque more consistent rather than periodic, at the cost of high-end power since straight blades get higher torque values, but didn't achieve the desired results. The manufacturing difficulty was with the blade thickness, as the 3d printers have a minimum thickness for design elements which the blade was under. To enable printing of the turbine the blade thickness was increased overall in a hope to preserve the desired shape.

The impulse turbine was modelled after the Pelton wheel but with some alterations as the impulse designs generally don't want to be submerged inside the water. The primary difficulty with the Pelton wheel is that the flow can only flow through a small part of the turbine without counteracting the torque. To control the water flow through the turbine part of it was blocked from the flow using the support structure as a shield, redirecting the flow either above the turbine or towards the turbine blades. By blocking part of the flow, the turbine could rotate as designed but some flow always passed through the turbine in the wrong direction, counteracting the generated torque. Compared to the reaction design, the manufacturing of the impulse turbine was easier since the detailed parts were thicker and could easily be printed. The disadvantage with the impulse design is its low efficiency. The tests showed that the tangential velocity was only 1/10 of the water flow velocity resulting in low RPM values. When including the flow blocked by the support structure in the efficient calculations the results worsen.

One problem that was for both types was the need of a surrounding support structure, resulting in smaller turbine radius. The need for the support was as the turbine have higher height than width would result in more force applied in the bottom compared to the top, bending or damaging the turbine.

8.3 Generator Conclusion

The generator designed was an axial flux permanent magnet synchronous generator (PMSG) over the more commonly radially used one. The advantage of the axial flux and why it was chosen over the radial one was the limited width and its higher magnetic flux density. An advantage for axial flux generator that was utilised was the removal of cores in the stator and rotor, making the construction easier as the can then be 3d printed. A focus when designing the generator was its efficiency and maximise the magnetic flux. Therefore, the area available on the rotor and stator were designed to be as concentrated on PM and coils as possible. The usage of the Halbach array for the rotor's magnets were a way to increase efficiency but the array has a minimum limit on the number of pole pairs. It was this reason why the cube magnets were chosen as eight of them could fit while also rotate to create the array. The winding types were chosen more as a practical choice rather than an optimal one as single layer concentrated winding was the only practical way to self wound coils on this scale, with diameter of around $1mm$. For similarly practical reasons were the coils chosen to be air cored rather than iron cored. To ensure maximum density of coils while being placed opposite the magnets, six slots could fit. To ensure a high winding factor, three phase connection were chosen.

To ensure a compact and simple design the generator was placed inside the turbine and its support structure. The rotor the top part of the turbine while the stator was in the roof of the support structure, opposite the rotor. This had several advantages, such as having fewer parts to produce and taking up less space making the design more compact. One of the largest advantages is the ease of waterproofing as the only accessible part would be the coil connections rather than the central axis.

The largest difficulty was always the distance between the rotor and stator as the PMs magnetic flux density rapidly weakens as distance increases and the high RPM values required. One problem was that the generator would be submerged in the water and to protect the magnets and coils a thin layer of waterproofing epoxy was applied on each side. The slots for the coils was closed off on the top apart from a small hole where the connections would go through since the stator was submerged. The problem with that design feature was the difference in 3d printing precision between different processes. The small openings could be printed in the reaction turbine parts by one manufacturer but not the impulse turbine by another. The same problem arose with the slots for the PMs where only one manufacturer could print with the required precision. This led to some problems for the impulse turbine and required workarounds which impacted the design. The problem with the rotor slot not working were solved by using a spare rotor from the reaction turbine parts, which resulted in a slight difference in radius of the turbine and rotor. For the stator the workaround required the coils connection ends to be brought on the outside of the structure. While not impacting the efficiency of the coils themselves this increased the gap between the rotor and stator slightly.

The reason why the generator failed to produce any measurable results is probably a combination of the low RPM values of the turbine together with the large gap between the rotor and stator. Of those the most important factor is the gap distance as once it exceeds $0.5mm$ the turbine losses most of its magnetic flux density.

8.4 Further Work

The area where most improvement could be made is the turbines as the generator's efficiency is not known. A different turbine design should be tested as there are few improvements possible for the tested designs. The cross-flow turbine design would be the next turbine type to test as it has a vertical axis, same as the tested impulse design, and it also utilises the entire surface area. Another design worth testing is a lightweight reaction type turbine with focus on high RPM. If the turbine can't achieve the required RPM for the axial flux turbine then a simple gearbox could be utilised but that would make it more complex and another part with losses. The general design of the support structure could also be improved but in general works very good as a template for future designs.

Bibliography

- [1] C. I. of Water and E. Management, “Water distribution system leakage in the uk,” 2015.
- [2] N. R. Council, *Drinking Water Distribution Systems: Assessing and Reducing Risks*. Washington, DC: The National Academies Press, 2006.
- [3] J. Chen, H. Yang, C. Liu, C. Lau, and M. Lo, “A novel vertical axis water turbine for power generation from water pipelines,” *Energy*, vol. 54, pp. 184 – 193, 2013.
- [4] D. Di Zenobio, K. Steenhaut, M. Celidonio, E. Sergio, and Y. Verbelen, “A self-powered wireless sensor for water/gas metering systems,” in *2012 IEEE International Conference on Communications (ICC)*, pp. 5772–5776, June 2012.
- [5] X. J. Li and P. H. J. Chong, “Design and implementation of a self-powered smart water meter,” *Sensors*, vol. 19, p. 4177, Sep 2019.
- [6] A. A. Pop, F. Jurca, C. Oprea, M. Chirca, S. Breban, and M. M. Radulescu, “Axial-flux vs. radial-flux permanent-magnet synchronous generators for micro-wind turbine application,” in *2013 15th European Conference on Power Electronics and Applications (EPE)*, pp. 1–10, Sep. 2013.
- [7] D. P. Arnold, F. Herrault, I. Zana, P. Galle, J.-W. Park, S. Das, J. H. Lang, and M. G. Allen, “Design optimization of an 8 w, microscale, axial-flux, permanent-magnet generator,” *Journal of Micromechanics and Microengineering*, vol. 16, pp. S290–S296, aug 2006.
- [8] O. Reynolds, “Xxix. an experimental investigation of the circumstances which determine whether the motion of water shall be direct or sinuous, and of the law of resistance in parallel channels,” *Philosophical Transactions of the Royal Society of London*, vol. 174, pp. 935–982, 1883.
- [9] D. E. D. E. U. M. U. R. K. R. S. J. W. Herbert Oertel, P. Erhard and K. Asfaw, *Prandtl-Essentials of Fluid Mechanics*, vol. 158 of *Applied Mathematical Sciences*. New York, NY: Springer New York, 2010.
- [10] P. Sritram and R. Suntivarakorn, “The effects of blade number and turbine baffle plates on the efficiency of free-vortex water turbines,” *IOP Conference Series: Earth and Environmental Science*, vol. 257, p. 012040, may 2019.

- [11] K. Gaywala, H. Shah, and P. Patel, “Performance prediction of a straight-bladed darrieus water turbine using multiple stream tube model,” *International Journal of Mechanical Engineering*, vol. 4, pp. 41–45, 06 2017.
- [12] H. Beri and Y. Yao, “Double multiple stream tube model and numerical analysis of vertical axis wind turbine,” *Energy and Power Engineering*, vol. 03, 01 2011.
- [13] M. O. L. Hansen and a. Hansen, Martin O. L., *Aerodynamics of wind turbines*. London: Routledge, [third edition]. ed., 2015.
- [14] A. Pendharkar, R. McGowan, K. Morillas, M. Pinder, and N. Komerath, “Optimization of a vertical axis micro wind turbine for low tip speed ratio operation,” 07 2012.
- [15] S. Brusca, R. Lanzafame, and M. Messina, “Design of a vertical-axis wind turbine: how the aspect ratio affects the turbine’s performance,” *International Journal of Energy and Environmental Engineering*, vol. 5, no. 4, pp. 333–340, 2014.
- [16] L. Battisti, A. Brightenti, E. Benini, and M. R. Castelli, “Analysis of different blade architectures on small VAWT performance,” *Journal of Physics: Conference Series*, vol. 753, p. 062009, sep 2016.
- [17] A. Alaimo, A. Esposito, A. Messineo, C. Orlando, and D. Tumino, “3d cfd analysis of a vertical axis wind turbine,” *Energies*, vol. 8, no. 4, pp. 3013–3033, 2015.
- [18] J. F. Gieras, *Axial flux permanent magnet brushless machines*. Dordrecht: Springer, 2nd ed. ed., 2008.
- [19] N. R. Skaar S. E., Krøvel Ø., “Distribution, coil-span and winding factors for pm machines with concentrated windings,” *Int. Conf. on Electr. Machines ICEM-2006*, 2006.
- [20] M. J. Kamper, R. Wang, and F. G. Rossouw, “Analysis and performance of axial flux permanent-magnet machine with air-cored nonoverlapping concentrated stator windings,” *IEEE Transactions on Industry Applications*, vol. 44, pp. 1495–1504, Sep. 2008.
- [21] F. Magnussen and C. Sadarangani, “Winding factors and joule losses of permanent magnet machines with concentrated windings,” in *IEEE International Electric Machines and Drives Conference, 2003. IEMDC’03.*, vol. 1, pp. 333–339 vol.1, June 2003.
- [22] T. D. Batzel, A. M. Skraba, and R. D. Massi, “Design and test of an ironless axial flux permanent magnet machine using halbach array,” in *Paper 088 , ENG-xxx*, 2014.
- [23] B. J. Cory, N. Jenkins, J. Ekanayake, G. Strbac, and B. M. Weedy, *Electric power systems*. Wiley, 5 ed., 2013.

- [24] Y.-b. Liang, L.-x. Zhang, E.-x. Li, X.-h. Liu, and Y. Yang, “Design considerations of rotor configuration for straight-bladed vertical axis wind turbines,” *Advances in Mechanical Engineering*, vol. 2014, pp. 1–15, 06 2014.
- [25] D. Jiyun, Y. Hongxing, S. Zhicheng, and G. Xiaodong, “Development of an inline vertical cross-flow turbine for hydropower harvesting in urban water supply pipes,” *Renewable Energy*, vol. 127, pp. 386 – 397, 2018.
- [26] I. Samora, V. Hasmatuchi, C. Münch-Alligné, M. J. Franca, A. J. Schleiss, and H. M. Ramos, “Experimental characterization of a five blade tubular propeller turbine for pipe inline installation,” *Renewable Energy*, vol. 95, pp. 356 – 366, 2016.
- [27] H. Raisigel, O. Cugat, and J. Delamare, “Permanent magnet planar micro-generators,” *Sensors and Actuators A: Physical*, vol. 130-131, pp. 438 – 444, 2006. Selected Papers from TRANSDUCERS ’05.

Appendix A

Design Schematics

The 3d models designed and used in this project can be found on git at <https://github.com/alexwillie/Energy-Harvesting-from-Water-Flow>.

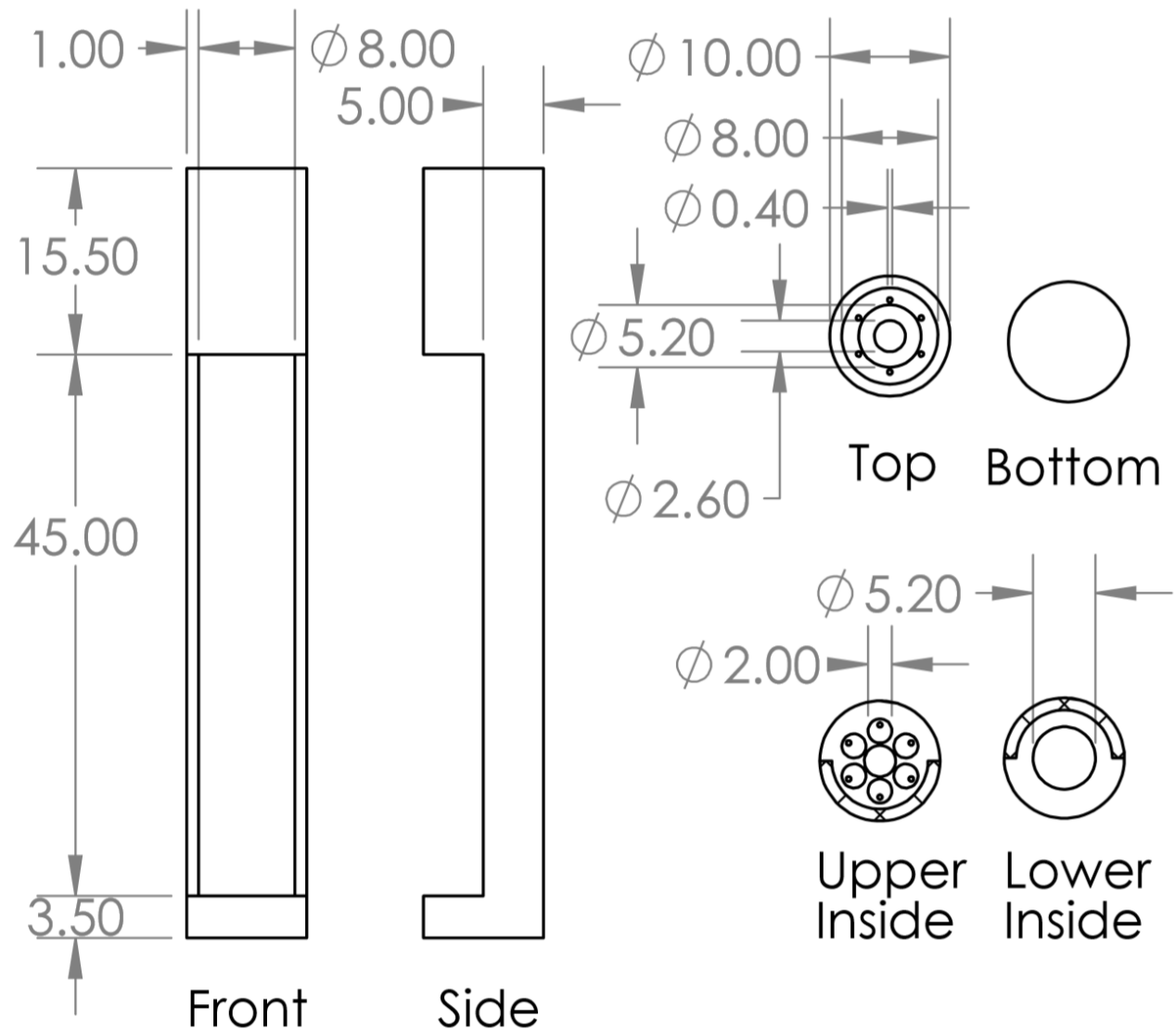


Figure A.1: Impulse turbine support structure design schematics in mm.

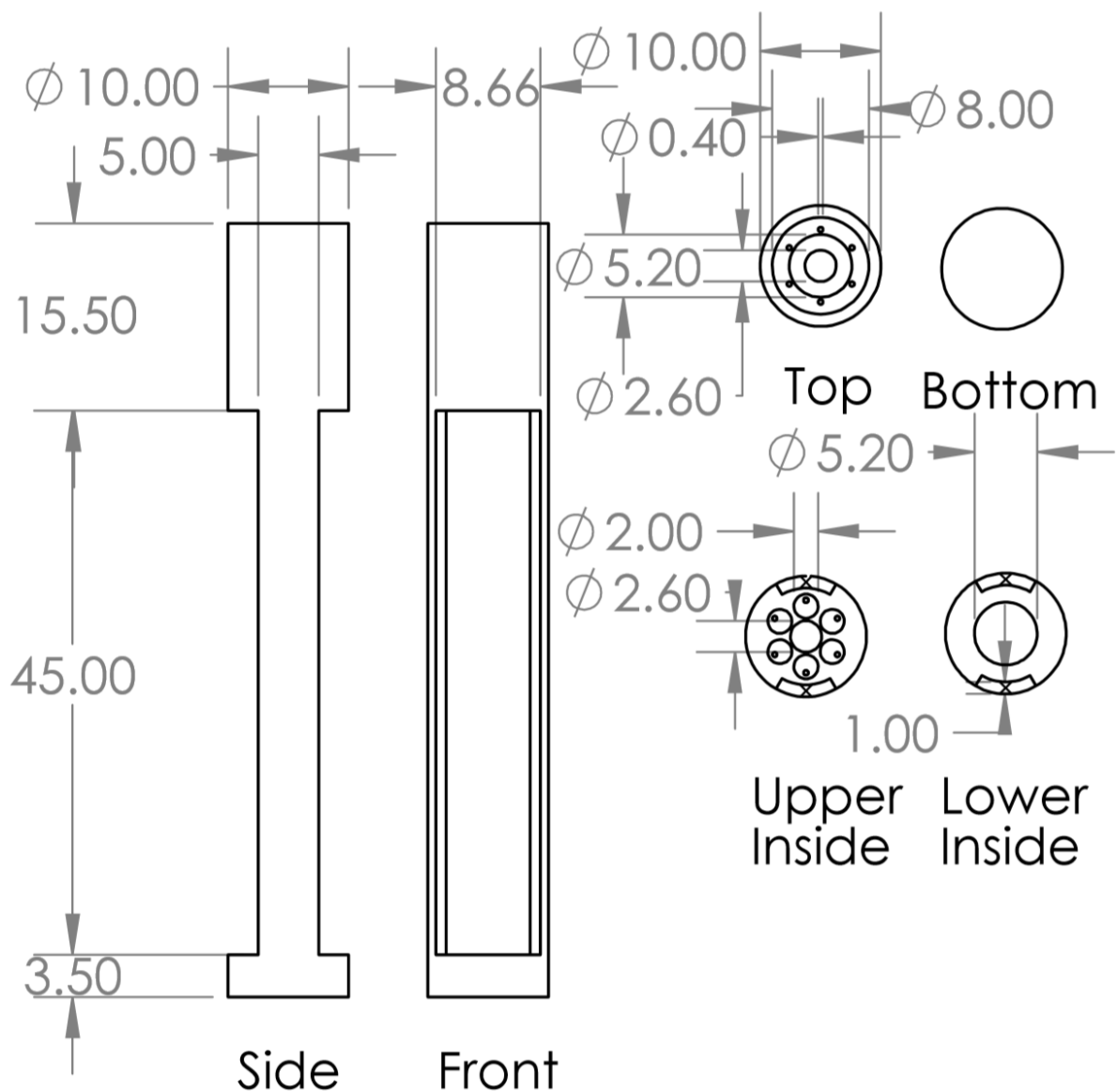


Figure A.2: Reaction turbine support structure design schematics in mm.

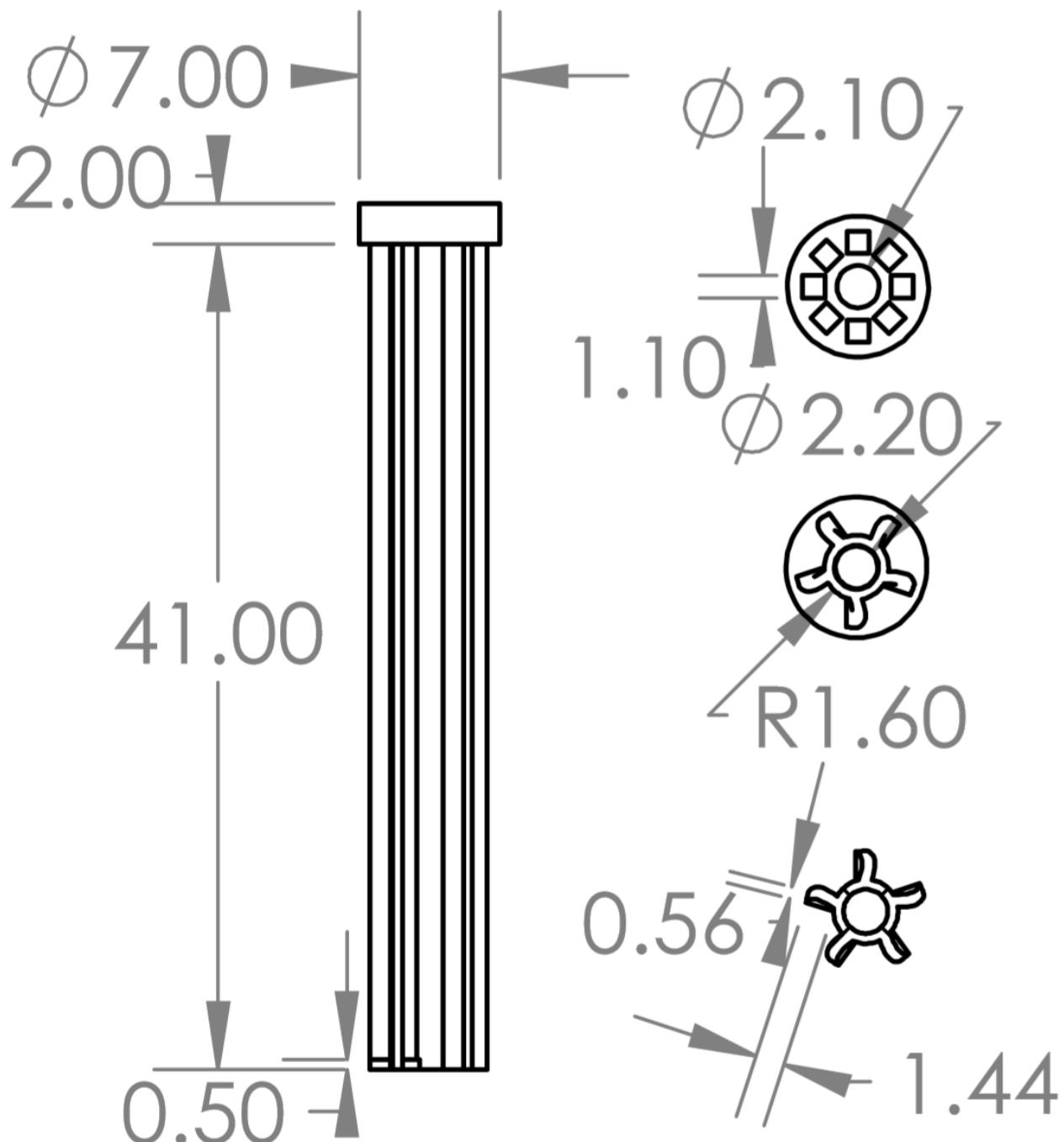


Figure A.3: Impulse turbine design schematics in mm.

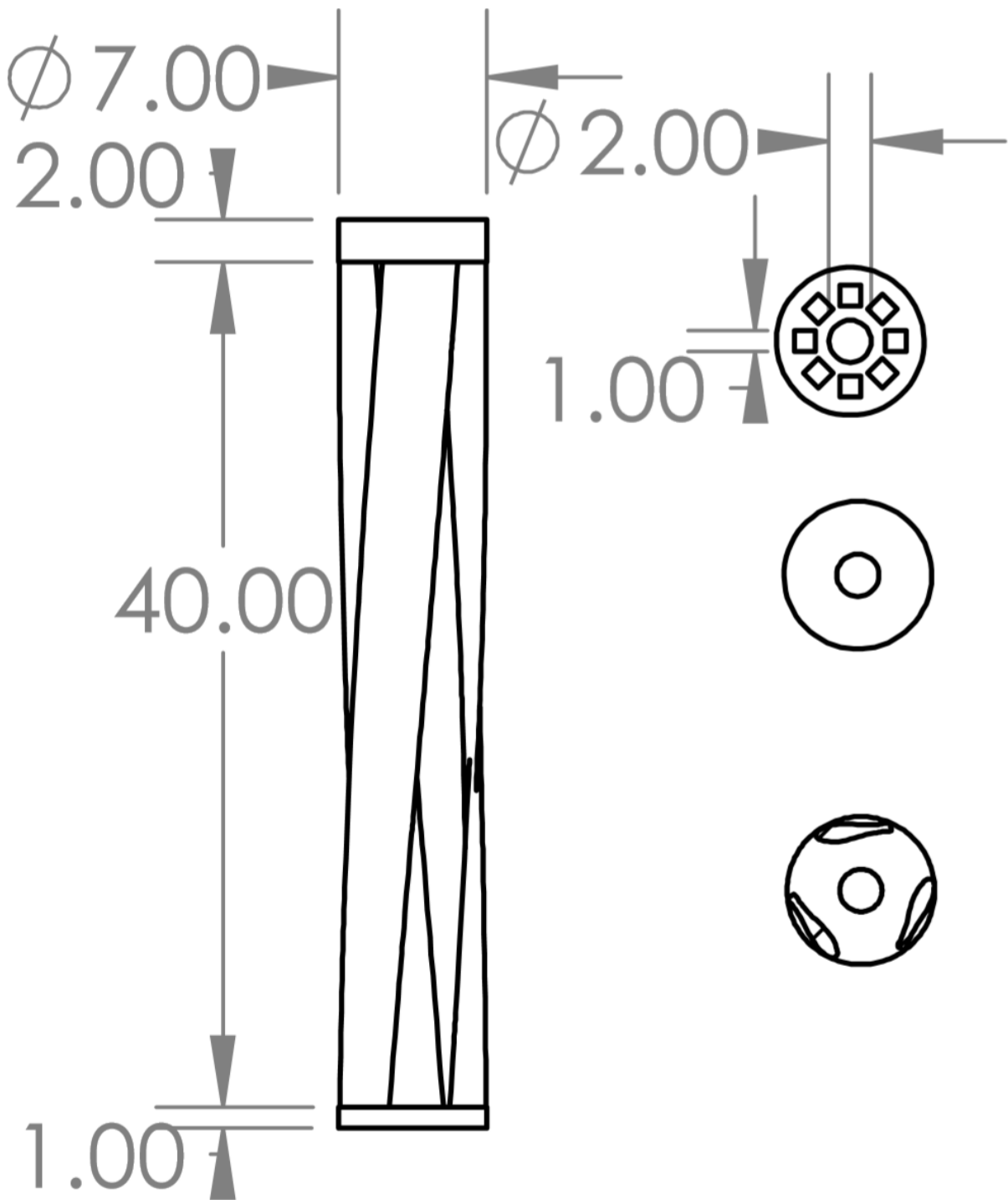


Figure A.4: Reaction turbine design schematics in mm.